arXiv:2603.10857v4 [q-fin.CP] 24 Sep 2026

SPX–VIX Risk Computations Via Perturbed Optimal Transport

Charlie Che**[1], Hanxuan Lin*†[2], Yudong Yang*‡[1], Guofan Hu*§[1], and Lei Fang*¶[1]

[1]Quantitative Trading & Research, JPMorganChase, New York, NY 10017, USA
[2]Quantitative Research China, JPMorganChase, Beijing, 100033, China

Abstract

We propose a model-independent framework for joint SPX–VIX derivatives risk generation using Perturbed Optimal Transport (POT). The calibrated Gibbs coupling induces an exponential family whose Fisher information governs the response to admissible market shocks. Exploiting this structure, we compute sensitivities for payoffs written on the calibrated state space via a single Fisher-based linear solve, replacing bump-and-recalibrate procedures. To capture VIX smile dynamics, we introduce a linearized Skew Stickiness Ratio (SSR) rule to propagate SPX-induced VIX future shifts to the full VIX smile, completing the VIX marginal component h_V of the perturbation vector. SSR determines how the VIX marginal target changes in response to an SPX shock, with second-order error control. We also identify a conditional coupling invariance that reduces the perturbed transport on (S_1, V, S_2) to an exact two-dimensional projection on (S_1, V), preserving martingality and variance consistency while lowering computational cost. Numerically, both the Fisher-based linear-response and the dimension-reduced method closely match full recalibration for VIX futures and VIX option cross-Greeks, yet are orders of magnitude faster. Hedging backtests show reduced hedged P&L variance versus a stochastic local-volatility benchmark, especially in volatile regimes. We further demonstrate that the framework extends beyond VIX vanilla options: a VIX-barrier forward-starting SPX call is priced and risked using the same Fisher linear solve, with the linear-response delta capturing a non-trivial sensitivity arising from variance-consistency recalibration even for a scale-invariant payoff. These results establish POT, coupled with linear response and SSR-based VIX smile propagation, as a practical, efficient framework for SPX–VIX risk propagation and hedging.

Keywords: SPX–VIX; perturbed optimal transport; entropic martingale optimal transport; Fisher information; linear response; dimensional reduction; Skew Stickiness Ratio (SSR); cross-Greeks; convex calibration; information geometry.

*charlie.che@jpmchase.com
†hanxuan.lin@jpmchase.com
‡yudong.yang@jpmchase.com
§guofan.hu@jpmchase.com
¶lei.x.fang@jpmchase.com

Notation

Symbol	Description
State spaces and dimension	
$\mathcal{S}_1 = \{s_1^1, \dots, s_1^{N_1}\}$	SPX grid at T_1
$\mathcal{S}_2 = \{s_2^1, \dots, s_2^{N_2}\}$	SPX grid at T_2
$\mathcal{V} = \{v^1, \dots, v^{N_V}\}$	VIX grid
$\mathcal{X} = \mathcal{S}_1 \times \mathcal{V} \times \mathcal{S}_2$	Full product state space
$\Delta(\mathcal{X})$	Probability simplex on $\mathcal{X}$
$K = N_1 + N_V + N_2 + 2N_1N_V$	Total parameter/statistic dimension
Time horizons	
T_1	First expiry (SPX and VIX)
T_2	Second SPX expiry
$\tau = T_2 - T_1$	Time interval ($\tau = 30$ days)
Probability measures and marginals	
$D(\mu\|\bar{\mu}) = \sum_x \mu \ln(\mu/\bar{\mu})$	KL divergence from $\bar{\mu}$ (minimized in MOT)
$\bar{\mu}(x) > 0$	Prior coupling on $\mathcal{X}$
μ_1, μ_V, μ_2	Target marginals for S_1, V, S_2
$\mathbf{m} = (\mu_1, \mu_V, \mu_2)$	Stacked marginal target vector
$\mu^\star$	Calibrated MOT optimal coupling
μ^ε	Perturbed coupling (shock size ε)
$\gamma^\star(s_1, v) := \sum_{s_2} \mu^\star(s_1, v, s_2)$	(S_1, V)-marginal of $\mu^\star$
γ^ε	Perturbed reduced coupling on $\mathcal{S}_1 \times \mathcal{V}$ (DR)
$\mu_2^{DR} = \sum_{s_1, v} \kappa^\star \gamma^\varepsilon$	Endogenous S_2 marginal under DR
$\kappa^\star(s_2 \mid s_1, v)$	Conditional kernel; fixed under Assumption 7.1
Constraint operators and admissible sets	
$\mathcal{A}_{\text{marg}}$	Marginal constraint operator
$\mathcal{A}_{\text{fin}}$	Financial constraint operator
$\mathcal{A} = (\mathcal{A}_{\text{marg}}; \mathcal{A}_{\text{fin}})$	Full stacked constraint operator
$\mathcal{P}$	3D MOT-admissible coupling set
$\mathcal{P}^\varepsilon$	Perturbed 3D admissible set (LR)
$\mathcal{Q}^\varepsilon$	Perturbed 2D admissible set (DR); see (54)
b_k	Constraint RHS ($b_k = (\mathbf{m})_k$ for marginal slots, $b_k = 0$ for financial slots)
$h = (h_1, h_V, h_2, \mathbf{0}) \in \mathbb{R}^K$	Full perturbation vector (financial slots zero); $\dot{b} = h$ (synonym, see (12))
$h_{\text{marg}} := (h_1, h_V, h_2)$	Marginal block of h

Symbol	Description
Dual parameters	
$\theta = (u_1, u_V, u_2, \{\Delta_M^{ij}\}, \{\Delta_C^{ij}\})$	Full gauge-fixed parameter vector
$u_1,\ u_V,\ u_2$	Marginal dual potentials
$a = e^{u_1},\ q = e^{u_V},\ c = e^{u_2}$	Sinkhorn scaling factors (Algorithm 1)
$q(v) = e^{u_V(v)}$	VIX Sinkhorn scaling factor (q replaces earlier b to avoid clash with constraint RHS b_k)
$\Delta_M(s_1, v)$	Delta-hedge Lagrange multiplier
$\Delta_C(s_1, v)$	Vega-hedge Lagrange multiplier
$\dot{\theta}^0 = d\theta^\varepsilon/d\varepsilon\|_{\varepsilon=0}$	First-order variation of $\theta^\star$
Sufficient statistics, log-partition, Fisher information	
$\{T_k\}_{k=1}^K$	Sufficient statistics (see (4))
$T^{\text{marg}},\ T^{\Delta_M},\ T^{\Delta_C}$	Marginal, delta, vega stat blocks
$\Lambda(\theta) = \ln \sum_x \bar{\mu}\, e^{\langle \theta, T \rangle}$	Log-partition function
$H = \nabla_\theta^2 \Lambda(\theta^\star) \succeq 0$	Fisher information matrix; $H \succ 0$ under Assumption 2.5
H^+	Moore–Penrose pseudoinverse; $H^+ = H^{-1}$ under Assumption 2.5
$H_{\text{marg}}, H_{MM}, H_{CC}, H_{MC}$	Diagonal blocks of H (see (11))
$H_{\text{marg},M}, H_{\text{marg},C}$	Off-diagonal coupling blocks of H
Payoffs, perturbations, and risk	
$L(x) = -\frac{2}{\tau} \ln x$	Log-return (VIX–variance link)
$\sigma_{\text{fwd}}^2 = \mathbb{E}_{\mu^\star}[L(S_2/S_1)]$	SPX-implied forward variance
$G : \mathcal{X} \to \mathbb{R}$	Payoff function
$\Pi(\varepsilon) = \mathbb{E}_{\mu^\varepsilon}[G]$	Model price under μ^ε
$(g_G)_k = \text{Cov}_{\mu^\star}(G, T_k)$	Payoff–statistic covariance; $g_G \in \text{range}(H)$
$\Psi = H^+ g_G$	Full influence vector
$\psi = (\psi_1, \psi_V, \psi_2)$	Marginal influence functions
SSR and VIX propagation	
δ_S	SPX spot bump size (§ 4.1)
δ_σ	SPX parallel vol bump size (§ 4.2)
δF_V	First-order VIX future shift
$A_{\text{SSR}}(v) = \partial_K^2 \Gamma\|_{K=v}$	SSR shape vector; $h_V = A_{\text{SSR}} \delta F_V$
$\Gamma(K)$	SSR sensitivity kernel (see (49))
$\mathsf{V}_{\text{SPX},i}^{BS}(K) := \partial_\sigma C_{BS}(S_0, K, T_i, \sigma)$	SPX Black-Scholes option vega at maturity T_i; see (32)
$\mathsf{V}_{\text{VIX}}^{BS}(K) := \partial_{\sigma_V} C_V(K)$	VIX option Black-Scholes vega
V_{SPX}	SPX vega (model-implied price sensitivity to SPX vol)
Skew Stickiness Ratio (SSR)	
$F,\ F_V$	SPX and VIX forward levels
$\sigma(K, F),\ \sigma_V(K, F_V)$	SPX and VIX implied volatilities
$S_{\log} = F\, \partial_K \sigma\|_{K=F}$	SPX ATM log-moneyness skew
$S_{\log,V} = F_V\, \partial_K \sigma_V\|_{K=F_V}$	VIX ATM log-moneyness skew
$\beta,\ \beta_V$	SPX and VIX Skew Stickiness Ratios

1 Introduction

Joint modeling of SPX and VIX derivatives has become a central problem in equity volatility markets. While SPX options encode the distribution of future equity prices, VIX options are derivative contracts written on VIX, the square root of forward variance. Consistency between these two markets is therefore essential for both pricing and risk management of the SPX/VIX derivative family.

Traditional approaches to the joint SPX–VIX modeling problem rely on parametric stochastic volatility models such as the Heston model, stochastic volatility with jumps, Bergomi model, or rough volatility frameworks Heston (1993); Gatheral (2006); Bergomi (2016); Bayer et al. (2023). Although these models provide tractable simulation dynamics, they impose structural assumptions on volatility dynamics that are not directly implied by the observed option surfaces. More fundamentally, traditional parametric continuous-time model struggle to simultaneously recover both the SPX and VIX marginals; practitioners therefore typically decouple the two surfaces, which means that cross-sensitivities between the SPX volatility surface and VIX derivatives are not captured at all.

More recently, several alternative approaches have been developed to address the joint SPX-VIX calibration problem beyond classical parametric stochastic-volatility models. Cuchiero et al.Cuchiero et al. (2025) propose a flexible signature based framework for joint SPX-VIX modeling and calibration, while Abi Jaber et al.Abi Jaber et al. (2023) introduce the quintic Ornstein-Uhlenbeck volatility model, which achieves accurate joint calibration through a parsimonious polynomial transformation of an Ornstein-Uhlenbeck factor. Moving away from prescribed parametric volatility dynamics, Guo et al. Guo et al. (2022) formulate joint SPX-VIX calibration through semimartingale optimal transport, constructing calibrated continuous-time models subject to the relevant market constraints. These developments illustrate a broader shift towards more flexible representations and optimization-based formulations of the joint calibration problems.

Partiuclarly relevant to the present work is the nonparametric approach of Guyon in Guyon (2020, 2024), who formulated the joint SPX–VIX calibration problem as a discrete martingale optimal transport (MOT) problem. In this framework the calibrated coupling between equity levels and forward variance is obtained by solving a discrete entropic optimal transport problem using Sinkhorn iterations Cuturi (2013); Benamou et al. (2015). The resulting Gibbs distribution exactly reproduces the observed SPX and VIX option prices while remaining free of parametric volatility assumptions.

While entropic martingale optimal transport provides an exact joint calibration of SPX and VIX smiles, calibration alone does not yield a practical risk framework. In existing implementations, sensitivities are typically obtained by re-running the full calibration after each market perturbation. This bump-and-recalibrate approach is both computationally expensive and obscures the structural relationship between market shocks and model-implied risk.

The central observation of this paper is that entropic martingale optimal transport naturally defines a statistical manifold whose local geometry determines how the calibrated coupling reacts to marginal perturbations. Because the optimal coupling belongs to an exponential family, its response to marginal shocks can be characterized by the Fisher information matrix of the calibrated Gibbs distribution. This perspective leads to a new framework, which we term *Perturbed Optimal Transport (POT)*, for risk generation without recalibration. Within this POT framework, we propose two distinct yet complementary methodologies: one leveraging the local geometry of the calibrated coupling via a Linear Response (LR) system derived from the Fisher information matrix, and another utilizing Dimensional Reduction (DR) to efficiently re-solve a simpler transport problem under specific conditional invariance assumptions.

Beyond providing analytic risk formulas, the POT framework also enables incorporating empirical volatility dynamics into the optimal transport formulation. In particular, we use the Skew Stickiness Ratio (SSR) dynamics for the VIX volatility surface to determine the VIX marginal component of the perturbation vector: an SPX perturbation shifts the VIX future via the forward-variance identity, and the linearized SSR rule then propagates this shift to the full VIX smile, specifying how the VIX marginal target μ_V changes. The constraint operator and dual structure are unchanged; only the right-hand side of the linear system, the perturbation vector $\dot{b}$, is updated. This allows the transport framework to incorporate empirically observed volatility smile dynamics without introducing parametric stochastic volatility models.

Taken together, these results establish Perturbed Optimal Transport (POT) as a unified framework for

joint calibration and risk propagation in SPX–VIX markets, offering efficient risk generation through both Linear Response and Dimensional Reduction techniques.

1.1 Related Literature

This work relates to two strands of literature.

Optimal transport in finance.

Martingale optimal transport has emerged as a model-free approach to derivative pricing and calibration Beiglböck et al. (2013); Henry-Labordère (2017). Guyon (2020, 2024) introduced an entropic optimal transport formulation for the joint calibration of SPX and VIX smiles, which can be solved efficiently using Sinkhorn iterations.

Computational optimal transport and entropy regularization.

Entropy-regularized transport problems have become widely used in machine learning and computational optimal transport due to their favorable numerical properties Cuturi (2013); Benamou et al. (2015); Peyré and Cuturi (2019). These formulations lead to Gibbs distributions whose structure enables efficient iterative algorithms.

Our contributions extend this literature by showing that entropic MOT calibration naturally induces a perturbation theory that can be used to generate risk sensitivities without recomputing the transport solution.

1.2 Main Contributions

The contributions of this paper are as follows.

1. **The Linear Response (LR) System For Perturbed Optimal Transport In SPX–VIX Markets.**

   We develop a perturbation framework for discrete entropic optimal transport under both marginal and financial constraints. Using the implicit function theorem applied to the dual formulation, we show that the calibrated Gibbs coupling depends smoothly on admissible market perturbations. This yields explicit linear-response formulas for sensitivities of arbitrary payoffs, governed by the Fisher information matrix of the calibrated exponential family.

2. **Linearized Skew Stickiness Ratio dynamics for VIX options.**

   We introduce a linearization of Skew Stickiness Ratio (SSR) dynamics for VIX implied volatility surfaces and use it to determine the VIX marginal component h_V of the perturbation vector: the SSR rule maps the SPX-induced VIX future shift to the full VIX smile change, updating the right-hand side $\dot{b}$ of the linear system while leaving the constraint operator unchanged. This formulation provides a model-independent mechanism for propagating SPX perturbations to the VIX volatility smile while preserving convexity and tractability of the entropic projection problem. The SSR linearization is compatible with both the perturbation-based linear-response risk engine and the dimension-reduced transport framework developed later in the paper.

3. **Dimensional Reduction (DR) Within The Perturbed Optimal Transport Framework.**

   We identify a conditional coupling invariance structure under which the perturbed three-dimensional transport problem on (S_1, V, S_2) reduces to a two-dimensional entropic projection on (S_1, V). Under this structure the conditional kernel of S_2 given (S_1, V) remains fixed, so martingality and variance-consistency constraints are automatically preserved. This reduction dramatically lowers the computational complexity of risk generation while maintaining financial consistency of the model.

4. **Empirical validation and hedging backtests.**

   We compare the LR and DR risk sensitivities against full recalibration of the SPX–VIX martingale optimal transport model across VIX futures and VIX option cross-Greeks, finding close agreement at

orders-of-magnitude lower computational cost. We further conduct hedging backtests on randomized VIX option portfolios; the transport-based hedges consistently achieve lower hedged P&L variance than a stochastic local volatility (SLV) benchmark, particularly during volatile market regimes. As a further demonstration, we price and risk a VIX-barrier forward-starting SPX call whose payoff depends jointly on V and S_2/S_1. Unlike VIX vanilla claims, this payoff cannot in general be valued from the calibrated marginals alone and therefore genuinely requires the joint SPX-VIX coupling. It provides a setting in which joint calibration and consequently perturbation of the joint transport plan is essential rather than merely a convenient route to cross-risk.

These contributions establish Perturbed Optimal Transport (POT) as a unified framework for SPX–VIX joint calibration, risk generation, and hedging. Throughout, the calibrated coupling is required to satisfy a martingale condition $\mathbb{E}[S_2 \mid S_1, V] = S_1$ and a variance-consistency condition $\mathbb{E}[L(S_2/S_1) \mid S_1, V] = V^2$; these structural conditions are defined formally in Section 2.

2 Mathematical Framework For Entropic Martingale Optimal Transport

2.1 Setup: State Space And Admissible Couplings

Let

$$\mathcal{S}_1 = \{s_1^1, \dots, s_1^{N_1}\}, \quad \mathcal{S}_2 = \{s_2^1, \dots, s_2^{N_2}\}, \quad \mathcal{V} = \{v^1, \dots, v^{N_V}\}$$

be finite state spaces for the SPX level at T_1, SPX level at T_2, and VIX level. Let $\mathcal{X} := \mathcal{S}_1 \times \mathcal{V} \times \mathcal{S}_2$, and let $\bar{\mu}(x) > 0$ be a strictly positive prior on $\mathcal{X}$. The target marginals $\mu_1 \in \Delta(\mathcal{S}_1)$, $\mu_V \in \Delta(\mathcal{V})$, $\mu_2 \in \Delta(\mathcal{S}_2)$ are extracted from observed SPX and VIX option prices.

In the SPX–VIX joint calibration problem, an admissible coupling must satisfy two kinds of linear constraints:

- **Marginal constraints** ($\mathcal{A}_{\text{marg}}$): μ reproduces the three prescribed marginals.
- **Financial constraints** ($\mathcal{A}_{\text{fin}}$): martingality of SPX and consistency between VIX and forward variance (Definition 2.1).

Both sets are linear in μ, so the *MOT-admissible set* is

$$\mathcal{P} = \big\{ \mu \in \Delta(\mathcal{X}) : \mathcal{A}_{\text{marg}}\mu = \mathbf{m}, \;\; \mathcal{A}_{\text{fin}}\mu = 0 \big\}, \tag{1}$$

where $\mathbf{m} = (\mu_1, \mu_V, \mu_2)$ stacks the marginal targets.

Definition 2.1 (Constraint operators: marginalisation and financial consistency). The linear operator $\mathcal{A}_{\text{marg}} : \mathbb{R}^{\mathcal{X}} \to \mathbb{R}^{N_1+N_V+N_2}$ marginalizes μ onto each coordinate axis:

$$\begin{aligned}
(\mathcal{A}_{\text{marg}}\mu)_1(s_1^i) &= \sum_{v,\, s_2} \mu(s_1^i, v, s_2), \\
(\mathcal{A}_{\text{marg}}\mu)_V(v^j) &= \sum_{s_1,\, s_2} \mu(s_1, v^j, s_2), \\
(\mathcal{A}_{\text{marg}}\mu)_2(s_2^k) &= \sum_{s_1,\, v} \mu(s_1, v, s_2^k).
\end{aligned}$$

The linear operator $\mathcal{A}_{\text{fin}} : \mathbb{R}^{\mathcal{X}} \to \mathbb{R}^{2N_1N_V}$ evaluates the conditional moment residuals at each node (s_1^i, v^j):

$$\begin{aligned}
(\mathcal{A}_{\text{fin}}\mu)^M_{ij} &= \sum_{s_2} \mu(s_1^i, v^j, s_2)\,(s_2 - s_1^i), && \textit{(martingale block)} \\
(\mathcal{A}_{\text{fin}}\mu)^C_{ij} &= \sum_{s_2} \mu(s_1^i, v^j, s_2)\,\big(L(s_2/s_1^i) - (v^j)^2\big). && \textit{(variance-consistency block)}
\end{aligned}$$

Writing $\mathcal{A} := (\mathcal{A}_{\text{marg}}; \mathcal{A}_{\text{fin}})$ and $b := (\mathbf{m}; 0) \in \mathbb{R}^{N_1+N_V+N_2+2N_1N_V}$, the admissible set (1) reads $\mathcal{P} = \{\mu \in \Delta(\mathcal{X}) : \mathcal{A}\mu = b\}$.

Remark (Financial interpretation of $\mathcal{A}_{\text{fin}}\mu = 0$). Setting $\mathcal{A}_{\text{fin}}\mu = 0$ imposes two families of conditions on the calibrated coupling, one per conditioning node (s_1^i, v^j):

1. **Martingale condition** ($(\mathcal{A}_{\text{fin}}\mu)_{ij}^M = 0$):

$$\mathbb{E}_\mu[S_2 \mid S_1 = s_1^i,\, V = v^j] \;=\; s_1^i,$$

   i.e. the SPX price is a risk-neutral martingale conditional on the SPX level and VIX index at T_1. We assume zero interest rates, dividends, and repos throughout, following Guyon (2020); with nonzero rates the condition becomes $\mathbb{E}[S_2/F_2 \mid S_1, V] = S_1/F_1$ where F_i is the forward price at T_i, and the grid is interpreted as normalized by the respective forwards.

2. **Variance-consistency condition** ($(\mathcal{A}_{\text{fin}}\mu)_{ij}^C = 0$):

$$\mathbb{E}_\mu\big[L(S_2/S_1) \mid S_1 = s_1^i,\, V = v^j\big] \;=\; (v^j)^2, \tag{2}$$

   i.e. the conditional expected log-contract payoff equals the VIX squared at T_1. This is the discrete form of Guyon's consistency condition Guyon (2020): by definition the VIX is the square root of the forward-realized variance of the SPX, so this identity must hold pointwise on the (S_1, V) grid.

Both conditions are linear in μ with zero right-hand side, confirming that the financial constraint targets in b are zero.

2.2 Entropic MOT: Primal–Dual Problem and Gibbs Form

We minimize relative entropy over the MOT-admissible set:

$$\mu^\star = \arg\inf_{\mu\in\mathcal{P}} D(\mu\|\bar\mu), \qquad D(\mu\|\bar\mu) = \sum_{x\in\mathcal{X}} \mu(x) \ln \frac{\mu(x)}{\bar\mu(x)}. \tag{3}$$

Sufficient statistics and log-partition function. The constraint operator $\mathcal{A}$ of Definition 2.1 and prior $\bar\mu$ determine the following sufficient statistics and log-partition function, which parametrize the exponential family of Gibbs couplings:

$$\{T_k\} = \underbrace{\{\mathbf{1}_{s_1=s_1^i},\, \mathbf{1}_{v=v^j},\, \mathbf{1}_{s_2=s_2^k}\}}_{\text{marginal indicators } T^{\text{marg}}} \cup \underbrace{\{\mathbf{1}_{(s_1,v)=(s_1^i,v^j)}\,(s_2 - s_1^i)\}_{i,j}}_{\text{delta payoffs } T^{\Delta_M}} \cup \underbrace{\{\mathbf{1}_{(s_1,v)=(s_1^i,v^j)}\,(L(s_2/s_1^i) - (v^j)^2)\}_{i,j}}_{\text{vega payoffs } T^{\Delta_C}}, \tag{4}$$

with full Lagrange multiplier vector $\theta = (u_1, u_V, u_2, \{\Delta_M^{ij}\}, \{\Delta_C^{ij}\}) \in \mathbb{R}^K$, where $\Delta_M^{ij} := \Delta_M(s_1^i, v^j)$ and $\Delta_C^{ij} := \Delta_C(s_1^i, v^j)$ are the node-indexed shorthand for the financial multipliers and log-partition function

$$\Lambda(\theta) = \ln \sum_{x\in\mathcal{X}} \bar\mu(x)\, e^{\langle\theta,\, T(x)\rangle}. \tag{5}$$

The two objects T and θ play distinct roles: $\{T_k\}$ are functions on $\mathcal{X}$: the row functions of $\mathcal{A}$, hence the generating set of its adjoint $\mathcal{A}^*$. The vector $\theta \in \mathbb{R}^K$ is the Lagrange multiplier for the constraint $\mathcal{A}\mu = b$; it lives in the codomain of $\mathcal{A}$ and is not a function on $\mathcal{X}$. The Gibbs exponent $(\mathcal{A}^*\theta)(x) = \langle\theta, T(x)\rangle$ is the pairing of these two objects.

Proposition 2.2 (Sufficient statistics as the adjoint of the constraint operator). Equip $\mathbb{R}^{\mathcal{X}}$ with the inner product $\langle f, g\rangle_{\mathcal{X}} := \sum_{x\in\mathcal{X}} f(x)g(x)$ and $\mathbb{R}^{N_1+N_V+N_2+2N_1N_V}$ with the standard Euclidean inner product. Let $\mathcal{A}$ be the operator of Definition 2.1 and $\{T_k\}$ the sufficient statistics of (4).

(i) $(\mathcal{A}\mu)_k = \langle T_k,\, \mu\rangle_{\mathcal{X}}$ for every index k.

(ii) The adjoint $\mathcal{A}^* : \mathbb{R}^{N_1+N_V+N_2+2N_1N_V} \to \mathbb{R}^{\mathcal{X}}$ satisfies

$$(\mathcal{A}^*\theta)(x) = \langle \theta,\, T(x)\rangle = \sum_k \theta_k\, T_k(x).$$

(iii) The KKT stationarity condition for (3) gives $\ln(\mu^\star/\bar{\mu}) = \mathcal{A}^*\theta^\star$ (up to an additive constant absorbed into the marginal-potential gauge), recovering the Gibbs form of the calibrated coupling.

Proof. (i) By Definition 2.1, each entry of $\mathcal{A}\mu$ is a sum over $x \in \mathcal{X}$ of $\mu(x)$ weighted by exactly one element of $\{T_k\}$. For instance, for the marginal index $k = (1, i)$:

$$(\mathcal{A}_{\text{marg}}\mu)_1(s_1^i) = \sum_{v,s_2} \mu(s_1^i, v, s_2) = \sum_{x\in\mathcal{X}} \mathbf{1}_{s_1(x)=s_1^i}\, \mu(x) = \langle T_{1,i},\, \mu\rangle_{\mathcal{X}}.$$

The same holds for every other index by inspection, so $(\mathcal{A}\mu)_k = \langle T_k, \mu\rangle_{\mathcal{X}}$ for all k.

(ii) By definition of the adjoint, $\langle \theta, \mathcal{A}\mu\rangle = \langle \mathcal{A}^*\theta, \mu\rangle_{\mathcal{X}}$ for all μ and θ. Using (i):

$$\langle \theta, \mathcal{A}\mu\rangle = \sum_k \theta_k\, (\mathcal{A}\mu)_k = \sum_k \theta_k\, \langle T_k, \mu\rangle_{\mathcal{X}} = \Big\langle \sum_k \theta_k T_k,\ \mu \Big\rangle_{\mathcal{X}}.$$

Since this holds for all μ, we identify $(\mathcal{A}^*\theta)(x) = \sum_k \theta_k T_k(x) = \langle \theta, T(x)\rangle$.

(iii) Stationarity of $\mathcal{L}(\mu, \theta) = D(\mu\|\bar{\mu}) - \langle \theta, \mathcal{A}\mu - b\rangle$ at $\mu^\star$ gives, for each $x \in \mathcal{X}$:

$$\left.\frac{\partial \mathcal{L}}{\partial \mu(x)}\right|_{\mu^\star} = \ln \frac{\mu^\star(x)}{\bar{\mu}(x)} + 1 - (\mathcal{A}^*\theta^\star)(x) = 0,$$

hence $\ln(\mu^\star(x)/\bar{\mu}(x)) = \langle \theta^\star, T(x)\rangle - 1$. The $+1$ arising from differentiating $D(\mu\|\bar{\mu})$ produces the constant -1 on the right-hand side above. Since $\sum_k T_{1,k}(x) \equiv 1$ on $\mathcal{X}$ (exactly one S_1-indicator fires at every x), the constant function -1 lies in range$(\mathcal{A}^*)$: it can be written as $\langle c, T(x)\rangle$ by setting $c_{1,k} = -1$ for all k and $c_j = 0$ otherwise. It is therefore absorbed into the marginal-potential component of $\theta^\star$, giving $\mu^\star(x) \propto \bar{\mu}(x)\, e^{\langle \theta^\star, T(x)\rangle}$. □

Theorem 2.3 (Existence, Uniqueness, and Gibbs Form). Assume:

(A1) $\bar{\mu}(x) > 0$ for all $x \in \mathcal{X}$;

(A2) $\mathcal{P} \neq \emptyset$;

(A3) there exists $\mu_0 \in \mathcal{P}$ with $\mu_0(x) > 0$ for all $x \in \mathcal{X}$ *(strictly positive feasible coupling).*

Then problem (3) has a unique minimizer $\mu^\star$ with $\mu^\star(x) > 0$ for all $x \in \mathcal{X}$, and it takes the *extended Gibbs form*

$$\mu^\star(s_1, v, s_2) \;\propto\; \bar{\mu}(s_1, v, s_2)\, \exp\Big(\underbrace{u_1(s_1) + u_V(v) + u_2(s_2)}_{\text{marginal potentials}} + \underbrace{\Delta_M(s_1, v)\,(s_2 - s_1)}_{\text{delta hedge}} + \underbrace{\Delta_C(s_1, v)\,\big(L(s_2/s_1) - v^2\big)}_{\text{vega hedge}}\Big), \tag{6}$$

where (u_1, u_V, u_2) are dual potentials for the marginal constraints and $\{\Delta_M(s_1, v),\, \Delta_C(s_1, v)\}$ are Lagrange multipliers for the financial constraints.

Proof. We follow the argument of Guyon Guyon (2020), Section 5, making each step explicit.

Existence and uniqueness. Since $\mathcal{X}$ is finite, $\Delta(\mathcal{X})$ is compact. With the convention $0 \ln 0 := 0$, the map $t \mapsto t \ln t$ is continuous on $[0, \infty)$, and $\bar{\mu}(x) > 0$ for every x ensures that $\mu \mapsto -\sum_x \mu(x) \ln \bar{\mu}(x)$ is continuous on $\Delta(\mathcal{X})$. Hence $D(\cdot \| \bar{\mu})$ is continuous on $\Delta(\mathcal{X})$. Strict convexity of $t \mapsto t \ln t$ on $[0, \infty)$ makes $\mu \mapsto \sum_x \mu(x) \ln \mu(x)$ strictly convex; adding the linear term $-\sum_x \mu(x) \ln \bar{\mu}(x)$ preserves strict convexity.

The feasible set $\mathcal{P} = \{\mu \in \Delta(\mathcal{X}) : \mathcal{A}\mu = b\}$ is the intersection of the simplex with an affine subspace, hence closed, convex, and compact; by hypothesis it is non-empty. Weierstrass's theorem gives a minimizer $\mu^\star$. If $\tilde{\mu}_1, \tilde{\mu}_2 \in \mathcal{P}$ were both minimizers with $\tilde{\mu}_1 \neq \tilde{\mu}_2$, then $\frac{1}{2}(\tilde{\mu}_1 + \tilde{\mu}_2) \in \mathcal{P}$ by convexity, and strict convexity of $t \mapsto t \ln t$ gives

$$D(\tfrac{1}{2}(\tilde{\mu}_1 + \tilde{\mu}_2) \,\|\, \bar{\mu}) < \tfrac{1}{2} D(\tilde{\mu}_1 \,\|\, \bar{\mu}) + \tfrac{1}{2} D(\tilde{\mu}_2 \,\|\, \bar{\mu}) = \min_{\mathcal{P}} D(\cdot \,\|\, \bar{\mu}).$$

This contradicts minimality of $\tilde{\mu}_1$ and $\tilde{\mu}_2$. Hence $\mu^\star$ is unique.

Strict positivity of $\mu^\star$. We show $\mu^\star(x) > 0$ for all x. Suppose for contradiction that $S^c := \{x \in \mathcal{X} : \mu^\star(x) = 0\}$ is nonempty. By (A3) there exists $\mu_0 \in \mathcal{P}$ with $\mu_0 > 0$ everywhere. For $t \in (0, 1]$, set $\mu_t := (1 - t)\mu^\star + t\mu_0 \in \mathcal{P}$ (by convexity of $\mathcal{P}$). Decompose $D(\mu_t \| \bar{\mu}) - D(\mu^\star \| \bar{\mu})$ into contributions from $S := \mathcal{X} \setminus S^c$ (where $\mu^\star > 0$, so $F(t) := \sum_{x \in S} \mu_t(x) \ln(\mu_t(x)/\bar{\mu}(x))$ is C^1 near $t = 0$) and from S^c:

$$D(\mu_t \| \bar{\mu}) - D(\mu^\star \| \bar{\mu}) \;=\; [F(t) - F(0)] + G(t),$$

where $G(t) := \sum_{x \in S^c} t\mu_0(x) \ln(t\mu_0(x)/\bar{\mu}(x))$. Expanding G using $\bar{\mu}(x) > 0$ on S^c,

$$G(t) \;=\; ct \ln t + O(t), \qquad c := \sum_{x \in S^c} \mu_0(x) > 0.$$

Since $F(t) - F(0) = O(t)$, we get $D(\mu_t \| \bar{\mu}) - D(\mu^\star \| \bar{\mu}) = ct \ln t + O(t) < 0$ for all sufficiently small $t > 0$, contradicting minimality of $\mu^\star$. Hence $S^c = \emptyset$ and $\mu^\star > 0$ everywhere.

Lagrangian and strong duality. Attach a multiplier θ to the equality constraint $\mathcal{A}\mu = b$ and form

$$\mathcal{L}(\mu, \theta) \;=\; D(\mu \| \bar{\mu}) - \langle \theta, \mathcal{A}\mu - b \rangle.$$

By Proposition 2.2(i)–(ii), $\langle \theta, \mathcal{A}\mu \rangle = \langle \mathcal{A}^* \theta, \mu \rangle = \mathbb{E}_\mu[\langle \theta, T \rangle]$, so

$$\mathcal{L}(\mu, \theta) \;=\; D(\mu \| \bar{\mu}) - \mathbb{E}_\mu[\langle \theta, T \rangle] + \langle \theta, b \rangle.$$

By (A3), $\mu_0 \in \mathcal{P}$ satisfies $\mu_0 > 0$, so $\mathcal{P} \cap \mathrm{ri}(\Delta(\mathcal{X})) \neq \emptyset$, where $\mathrm{ri}(\Delta(\mathcal{X})) = \{\mu : \mu(x) > 0 \ \forall x\}$ denotes the relative interior of the simplex. This is precisely Slater's condition for the equality-constrained program with $\Delta(\mathcal{X})$ as the ambient domain: it guarantees strong duality and that the dual supremum is attained at finite $\theta^\star$ (finite-dimensional convex duality; see Rockafellar (1970), Thm. 28.2). The minimax theorem (applied to $\mathcal{L}$, which is convex in μ and linear in θ) then yields no duality gap:

$$\min_{\mu \in \mathcal{P}} D(\mu \| \bar{\mu}) \;=\; \sup_{\theta} \; g(\theta), \qquad g(\theta) \;:=\; \inf_{\mu \in \Delta(\mathcal{X})} \mathcal{L}(\mu, \theta). \tag{7}$$

Donsker–Varadhan evaluation of the inner infimum. Fix θ and set $X(x) := \langle \theta, T(x) \rangle$. Define the tilted measure

$$\mu_\theta(x) \;:=\; \frac{\bar{\mu}(x)\, e^{X(x)}}{\mathbb{E}_{\bar{\mu}}[e^X]} \;=\; \bar{\mu}(x)\, e^{X(x) - \Lambda(\theta)},$$

using (5) in the second equality. For any $\mu \in \Delta(\mathcal{X})$, the identity $\ln(\mu(x)/\bar{\mu}(x)) = \ln(\mu(x)/\mu_\theta(x)) + X(x) - \Lambda(\theta)$ gives, after summing against μ,

$$D(\mu \| \bar{\mu}) - \mathbb{E}_\mu[X] \;=\; D(\mu \| \mu_\theta) - \Lambda(\theta).$$

Since $D(\mu \| \mu_\theta) \geq 0$ with equality iff $\mu = \mu_\theta$, the infimum over $\mu \in \Delta(\mathcal{X})$ equals $-\Lambda(\theta)$ and is attained uniquely at μ_θ. Substituting into (7),

$$g(\theta) \;=\; \langle \theta, b \rangle - \Lambda(\theta),$$

which is concave in θ (as Λ is convex, being a log-sum-exp).

Gibbs form. Since the problem is finite-dimensional, the primal optimum $\mu^\star$ is attained (proved above) and strong duality holds (7). By the KKT theorem for convex programs with linear equality constraints, there exists a multiplier $\theta^\star \in \mathbb{R}^K$ satisfying the stationarity condition $\nabla_\mu \mathcal{L}(\mu^\star, \theta^\star) = 0$; this $\theta^\star$ attains the dual supremum. At any such $\theta^\star$, the inner infimum defining $g(\theta^\star)$ is uniquely attained at $\mu_{\theta^\star}$ (as shown above); strong duality then forces $\mu^\star = \mu_{\theta^\star}$, giving

$$\mu^\star(x) \;\propto\; \bar{\mu}(x)\, \exp\big(\langle \theta^\star, T(x)\rangle\big).$$

Expanding $\langle \theta^\star, T(x)\rangle$ block by block via (4) and Definition 2.1, with $x = (s_1, v, s_2)$:

$$\langle \theta^\star, T(x)\rangle \;=\; u_1(s_1) + u_V(v) + u_2(s_2) + \Delta_M(s_1, v)(s_2 - s_1) + \Delta_C(s_1, v)\big(L(s_2/s_1) - v^2\big),$$

where u_1, u_V, u_2 are the Lagrange multipliers for the marginal constraints $\mathcal{A}_{\text{marg}}\mu = \mathbf{m}$, and Δ_M, Δ_C are the Lagrange multipliers for the financial constraints $\mathcal{A}_{\text{fin}}\mu = 0$. This is exactly (6). □

Financial interpretation of the dual multipliers.

- $\Delta_M(s_1, v)$ is the *delta hedge multiplier*: it prices the conditional forward payoff $s_2 - s_1$ at each node (s_1, v), enforcing $\mathbb{E}[S_2 \mid S_1, V] = S_1$.
- $\Delta_C(s_1, v)$ is the *vega hedge multiplier*: it prices the conditional log-contract payoff $L(s_2/s_1) - v^2$ at each node (s_1, v), enforcing $\mathbb{E}[L(S_2/S_1) \mid S_1, V] = V^2$.

Their values are determined by the Newton/LM inner loop of Algorithm 1.

Corollary 2.4 (Dual Objective and Optimality Conditions). The optimal value of (3) equals

$$\sup_\theta \Big\{ \langle \mathbf{m},\, \theta_{\text{marg}} \rangle - \Lambda(\theta) \Big\},$$

where $\theta_{\text{marg}} = (u_1, u_V, u_2)$ and the financial components (Δ_M, Δ_C) enter only through $\Lambda(\theta)$. The supremum is attained at $\theta^\star$ whose first-order conditions are

$$\frac{\partial \Lambda}{\partial \theta_k}(\theta^\star) = b_k \quad \forall\, k, \tag{8}$$

where $b_k = \mathbf{m}_k$ for marginal components and $b_k = 0$ for financial components. Equation (8) is precisely $\mathbb{E}_{\mu^\star}[T_k] = b_k$, i.e., the calibrated coupling matches all constraints.

Proof. We derive the dual formula, establish the first-order conditions at the optimum, and interpret them block by block following Guyon Guyon (2020), eq. (5.8).

Dual objective. From the proof of Theorem 2.3, strong duality holds and the dual function is

$$g(\theta) \;=\; \inf_{\mu \in \Delta(\mathcal{X})} \mathcal{L}(\mu, \theta) \;=\; \langle \theta, b\rangle - \Lambda(\theta).$$

Since $b = (\mathbf{m}; 0)$, the inner product splits as $\langle \theta, b\rangle = \langle \theta_{\text{marg}}, \mathbf{m}\rangle + \langle \theta_{\text{fin}}, 0\rangle = \langle \mathbf{m}, \theta_{\text{marg}}\rangle$, so the dual problem is

$$D(\mu^\star \| \bar{\mu}) \;=\; \sup_\theta \big\{ \langle \mathbf{m}, \theta_{\text{marg}}\rangle - \Lambda(\theta) \big\}, \tag{9}$$

with g concave (as Λ is convex).

First-order conditions. Since the dual supremum is attained at $\theta^\star$ (Theorem 2.3) and g is differentiable, $\nabla_\theta g(\theta^\star) = 0$, i.e.

$$b_k \;=\; \frac{\partial \Lambda}{\partial \theta_k}(\theta^\star) \qquad \forall\, k. \tag{10}$$

Mean-parameterization identity. Differentiating $\Lambda(\theta) = \ln \sum_x \bar{\mu}(x) e^{\langle \theta, T(x) \rangle}$ with respect to θ_k gives

$$\frac{\partial \Lambda}{\partial \theta_k}(\theta) = \frac{\sum_x T_k(x)\, \bar{\mu}(x)\, e^{\langle \theta, T(x) \rangle}}{\sum_x \bar{\mu}(x)\, e^{\langle \theta, T(x) \rangle}} = \mathbb{E}_{\mu_\theta}[T_k],$$

where $\mu_\theta(x) \propto \bar{\mu}(x) e^{\langle \theta, T(x) \rangle}$. At the dual optimum $\mu_{\theta^\star} = \mu^\star$ (Theorem 2.3), so (10) becomes

$$\mathbb{E}_{\mu^\star}[T_k] \;=\; b_k \qquad \forall\, k,$$

which is exactly (8).

Block-wise interpretation. Reading (8) block by block via (4):

- *Marginal block* $(k = (1,i), (V,j), (2,k'))$: $\mathbb{E}_{\mu^\star}[\mathbf{1}_{s_1 = s_1^i}] = \mu_1(s_1^i)$, $\mathbb{E}_{\mu^\star}[\mathbf{1}_{v = v^j}] = \mu_V(v^j)$, $\mathbb{E}_{\mu^\star}[\mathbf{1}_{s_2 = s_2^{k'}}] = \mu_2(s_2^{k'})$: the calibrated coupling reproduces the three prescribed marginals.
- *Delta block* $(k = (M,i,j))$: $\mathbb{E}_{\mu^\star}\big[\mathbf{1}_{(s_1,v) = (s_1^i, v^j)}(s_2 - s_1^i)\big] = 0$: the martingale condition holds at every node (s_1^i, v^j).
- *Vega block* $(k = (C,i,j))$: $\mathbb{E}_{\mu^\star}\big[\mathbf{1}_{(s_1,v) = (s_1^i, v^j)}(L(s_2/s_1^i) - (v^j)^2)\big] = 0$: the variance-consistency condition holds at every node (s_1^i, v^j).

Together these confirm that $\mu^\star \in \mathcal{P}$, so the calibrated coupling matches all constraints simultaneously. □

2.3 Gauge Fixing And Numerical Stability

The marginal potentials (u_1, u_V, u_2) are not uniquely determined. Adding constants (c_1, c_V, c_2) with $c_1 + c_V + c_2 = 0$ leaves the unnormalized Gibbs weights $\bar{\mu}(x) e^{\langle \theta, T(x) \rangle}$ unchanged; equivalently, since the normalization factor $Z(\theta)$ scales by $e^{c_1 + c_V + c_2}$, the *normalized* coupling (6) is invariant under *any* constant shift (c_1, c_V, c_2). The two-dimensional gauge freedom is confined to the marginal block; the financial multipliers $\Delta_M(s_1, v)$ and $\Delta_C(s_1, v)$ are *uniquely determined* by the financial constraints at each node (s_1^i, v^j) and carry no gauge ambiguity.

To fix the gauge in the marginal block we impose

$$\sum_{s_1} \mu_1(s_1)\, u_1(s_1) = 0, \qquad \sum_{v} \mu_V(v)\, u_V(v) = 0.$$

Under this fixing, the full gauge-fixed parameter vector is

$$\theta \;\in\; \mathbb{R}^{(N_1 + N_V + N_2 - 2) \,+\, 2N_1 N_V},$$

where $N_1 + N_V + N_2 - 2$ degrees of freedom come from the gauge-fixed marginal potentials and $2N_1 N_V$ from the financial multipliers $\{\Delta_M^{ij}, \Delta_C^{ij}\}$.

2.4 Fisher Information: Hessian of the Log-Partition and Covariance of Dual Basis Functions

We now prove the central identity that underlies the perturbation theory, and state the non-degeneracy condition under which H is strictly positive definite.

Assumption 2.5 (Conditional non-degeneracy). For every node $(s_1^i, v^j) \in \mathcal{S}_1 \times \mathcal{V}$, the conditional distribution $\mu_{ij}^\star(\cdot) := \mu^\star(\cdot \mid s_1^i, v^j)$ has support of cardinality ≥ 3, and the three functions $\{1,\ s_2 - s_1^i,\ L(s_2/s_1^i) - (v^j)^2\}$ are linearly independent on $\mathrm{supp}(\mu_{ij}^\star)$.

Remark. Assumption 2.5 is a condition on the grid, not on the coupling: it holds whenever $|\mathcal{S}_2| \geq 3$ and no three points in $\mathcal{S}_2$ satisfy an exact affine relation involving the delta and vega payoff kernels. Since $\bar{\mu} > 0$ forces $\mu^\star > 0$ on $\mathcal{X}$, the full support condition $|\mathrm{supp}(\mu^\star_{ij})| = |\mathcal{S}_2|$ is automatic; the affine-independence part is a mild regularity condition satisfied by any generic grid. In practice (and in the numerical experiments of Section 8), Assumption 2.5 holds, and H is strictly positive definite. When it fails at isolated nodes, H is positive semi-definite and the Moore–Penrose pseudoinverse H^+ replaces H^{-1} throughout; all downstream results remain valid (see Lemmas 2.7 and 2.8 below).

Log-partition function and invertibility of H. On the gauge-fixed parameter space, $\Lambda(\theta)$ is C^∞. Its Hessian $H = \nabla^2_\theta \Lambda(\theta^\star)$ coincides with the Fisher information matrix of the calibrated exponential family. H is positive semi-definite in general; under Assumption 2.5 above, H is strictly positive definite and the linear response system has a unique solution. The Moore–Penrose pseudoinverse H^+ is used throughout; under Assumption 2.5, $H^+ = H^{-1}$.

Proposition 2.6 (Fisher Information = Hessian of Λ = Covariance of T). Let θ be the gauge-fixed MOT parameter vector, $\{T_k\}$ the sufficient statistics (4), and $\mu_\theta(x) \propto \bar{\mu}(x) \exp\langle \theta, T(x)\rangle$. Then:

(i) *(Mean parameterization)* $\dfrac{\partial \Lambda}{\partial \theta_k} = \mathbb{E}_{\mu_\theta}[T_k]$.

(ii) *(Fisher information as Hessian and covariance)* $H_{kl} := \dfrac{\partial^2 \Lambda}{\partial \theta_k \, \partial \theta_l} = \mathrm{Cov}_{\mu_\theta}(T_k, T_l)$.

In particular $H = \nabla^2_\theta \Lambda \succeq 0$. Under Assumption 2.5, $H \succ 0$ on the gauge-fixed subspace.

Proof. Write the partition function and log-partition function explicitly:

$$Z(\theta) \;=\; \sum_{x \in \mathcal{X}} \bar{\mu}(x)\, e^{\langle \theta,\, T(x)\rangle}, \qquad \Lambda(\theta) = \ln Z(\theta).$$

For $x = (s_1, v, s_2)$, expanding $\langle \theta, T(x)\rangle$ block by block via (4):

$$\langle \theta, T(x)\rangle \;=\; u_1(s_1) + u_V(v) + u_2(s_2) \;+\; \Delta_M(s_1, v)\,(s_2 - s_1) \;+\; \Delta_C(s_1, v)\,\big(L(s_2/s_1) - v^2\big),$$

so $Z(\theta) = \sum_{s_1, v, s_2} \bar{\mu}(s_1, v, s_2)\, e^{\langle \theta, T(x)\rangle}$ and the Gibbs measure is $\mu_\theta(x) = \bar{\mu}(x)\, e^{\langle \theta, T(x)\rangle}/Z(\theta)$.

Part (i): gradient of Λ. Differentiating $\Lambda = \ln Z$ with respect to θ_k by the chain rule:

$$\frac{\partial \Lambda}{\partial \theta_k}(\theta) \;=\; \frac{1}{Z(\theta)} \frac{\partial Z(\theta)}{\partial \theta_k}.$$

Since $T_k(x)$ multiplies $e^{\langle \theta, T(x)\rangle}$ when differentiating with respect to θ_k,

$$\frac{\partial Z(\theta)}{\partial \theta_k} \;=\; \sum_{x \in \mathcal{X}} \bar{\mu}(x)\, T_k(x)\, e^{\langle \theta, T(x)\rangle}.$$

Dividing through by $Z(\theta)$ recognizes each term as $\mu_\theta(x)$:

$$\frac{\partial \Lambda}{\partial \theta_k}(\theta) \;=\; \sum_{x \in \mathcal{X}} T_k(x) \underbrace{\frac{\bar{\mu}(x)\, e^{\langle \theta, T(x)\rangle}}{Z(\theta)}}_{\mu_\theta(x)} \;=\; \mathbb{E}_{\mu_\theta}[T_k].$$

Part (ii): Hessian of Λ. Differentiate $\partial\Lambda/\partial\theta_k = \mathbb{E}_{\mu_\theta}[T_k] = \sum_x T_k(x)\mu_\theta(x)$ with respect to θ_l:

$$\frac{\partial^2\Lambda}{\partial\theta_k\,\partial\theta_l} \;=\; \sum_{x\in\mathcal{X}} T_k(x)\,\frac{\partial\mu_\theta(x)}{\partial\theta_l}.$$

From $\mu_\theta(x) = \bar{\mu}(x)e^{\langle\theta,T(x)\rangle}/Z(\theta)$,

$$\frac{\partial\mu_\theta(x)}{\partial\theta_l} \;=\; \mu_\theta(x)\Big(T_l(x) - \frac{\partial\Lambda}{\partial\theta_l}\Big) \;=\; \mu_\theta(x)\big(T_l(x) - \mathbb{E}_{\mu_\theta}[T_l]\big).$$

Substituting and splitting the sum:

$$\begin{aligned}\frac{\partial^2\Lambda}{\partial\theta_k\,\partial\theta_l} \;&=\; \sum_x T_k(x)\,\mu_\theta(x)\big(T_l(x) - \mathbb{E}_{\mu_\theta}[T_l]\big)\\ &=\; \sum_x T_k(x)\,T_l(x)\,\mu_\theta(x) \;-\; \mathbb{E}_{\mu_\theta}[T_l]\sum_x T_k(x)\,\mu_\theta(x)\\ &=\; \mathbb{E}_{\mu_\theta}[T_kT_l] \;-\; \mathbb{E}_{\mu_\theta}[T_k]\,\mathbb{E}_{\mu_\theta}[T_l] \;=\; \mathrm{Cov}_{\mu_\theta}(T_k,T_l).\end{aligned}$$

Positive semi-definiteness. For any $c\in\mathbb{R}^K$,

$$c^\top Hc \;=\; \mathrm{Var}_{\mu_\theta}\big(\langle c,T\rangle\big) \;\geq\; 0,$$

so $H\succeq 0$. Equality holds iff $\sum_k c_kT_k(x)$ is constant on $\mathcal{X}$, i.e. $c\in\ker(H)$. Under Assumption 2.5 the three functions $\{1, s_2-s_1^i, L(s_2/s_1^i)-(v^j)^2\}$ are linearly independent on each fiber, so no non-trivial combination in $\mathbb{R}^K$ is constant; together with gauge fixing, this forces $c=0$, giving $H\succ 0$. □

Lemma 2.7 (Payoff covariances lie in range(H)). For any payoff $G:\mathcal{X}\to\mathbb{R}$, the covariance vector $g_G := \mathrm{Cov}_{\mu^\star}(G,T)\in\mathbb{R}^K$ satisfies $g_G\in\mathrm{range}(H)$.

Proof. If $c\in\ker(H)$ then $\sum_k c_kT_k\equiv\gamma$ on $\mathcal{X}$, so $c^\top g_G = \mathrm{Cov}_{\mu^\star}(G,\gamma) = 0$. Hence $g_G\perp\ker(H) = \mathrm{range}(H)^\perp$. □

Lemma 2.8 (Admissible perturbations lie in range(H)). Let $\dot{b}=(h_1,h_V,h_2,0,\dots,0)\in\mathbb{R}^K$ be a marginal perturbation satisfying the mass-conservation conditions $\sum_{s_1}h_1 = \sum_v h_V = \sum_{s_2}h_2 = 0$. Then $\dot{b}\in\mathrm{range}(H)$, so $H\dot{\theta}^0=\dot{b}$ is solvable.

Proof. Any $c\in\ker(H)$ has its marginal block of the form $(\gamma_1\mathbf{1},\gamma_V\mathbf{1},\gamma_2\mathbf{1})$ with $\gamma_1+\gamma_V+\gamma_2=0$ (from the gauge structure). Then $c^\top\dot{b} = \gamma_1\sum h_1+\gamma_V\sum h_V+\gamma_2\sum h_2 = 0$ by mass conservation, so $\dot{b}\perp\ker(H)$. □

Remark. This identity encodes three equivalent viewpoints on H: (a) *curvature of the dual* H measures how sharply the dual objective curves at the optimum; (b) *spread of the dual basis functions* H_{kl} is the covariance of the sufficient statistics T_k and T_l under the calibrated Gibbs measure; (c) *Riemannian metric-* H is the Fisher–Rao metric on the statistical manifold of calibrated couplings. The linear response formula $\Pi'(0) = g^\top H^+h$ (Theorem 3.5) is the statement that marginal perturbations h project onto the tangent space of this manifold via H^+.

Block structure of the MOT Fisher matrix. Partitioning H according to $\theta=(u,\Delta_M,\Delta_C)$ gives

$$H = \begin{pmatrix} H_{\mathrm{marg}} & H_{\mathrm{marg},M} & H_{\mathrm{marg},C}\\ H_{M,\mathrm{marg}} & H_{MM} & H_{MC}\\ H_{C,\mathrm{marg}} & H_{CM} & H_{CC}\end{pmatrix}, \tag{11}$$

where $\mu^\star_{ij}$ denotes the conditional distribution of s_2 given $(s_1, v) = (s_1^i, v^j)$, and the financial diagonal blocks are block-diagonal:

$$\begin{aligned}(H_{MM})_{ij,kl} &= \mathbf{1}_{(i,j)=(k,l)}\ \mathrm{Var}_{\mu^\star_{ij}}(s_2 - s_1^i),\\ (H_{CC})_{ij,kl} &= \mathbf{1}_{(i,j)=(k,l)}\ \mathrm{Var}_{\mu^\star_{ij}}\big(L(s_2/s_1^i) - (v^j)^2\big),\\ (H_{MC})_{ij,kl} &= \mathbf{1}_{(i,j)=(k,l)}\ \mathrm{Cov}_{\mu^\star_{ij}}\big(s_2 - s_1^i,\ L(s_2/s_1^i) - (v^j)^2\big).\end{aligned}$$

The block-diagonal structure of H_{MM} and H_{CC} reflects the node-local support of the financial payoffs; only the off-diagonal blocks $H_{\mathrm{marg},M}$ and $H_{\mathrm{marg},C}$ couple the marginal and financial directions.

3 Perturbation Theory: General Marginal Shocks

3.1 Admissible Perturbations

Let $\mu^\star$ be the unique MOT optimizer of Section 2. Risk generation requires understanding how $\mu^\star$ responds to changes in market data. In the SPX–VIX setting, market perturbations affect the *marginal* constraints (changing option prices shifts μ_1, μ_V, μ_2) while the *financial* constraints (martingality and variance consistency) are structural and remain fixed.

A *directional marginal perturbation* specifies component functions

$$h_1 : \mathcal{S}_1 \to \mathbb{R}, \quad h_V : \mathcal{V} \to \mathbb{R}, \quad h_2 : \mathcal{S}_2 \to \mathbb{R},$$

satisfying the mass-preserving constraints

$$\textstyle\sum_{s_1} h_1(s_1) = 0, \quad \sum_v h_V(v) = 0, \quad \sum_{s_2} h_2(s_2) = 0.$$

For ε sufficiently small, the perturbed marginals $\mu_i^\varepsilon = \mu_i + \varepsilon h_i$ remain in the interior of the simplex. In the full parameter space $\theta = (u_1, u_V, u_2, \{\Delta_M^{ij}\}, \{\Delta_C^{ij}\})$ this corresponds to the full perturbation vector

$$h \ := \ \big(h_1,\, h_V,\, h_2,\, \underbrace{0, \ldots, 0}_{2N_1N_V}\big) \ \in \mathbb{R}^K, \tag{12}$$

i.e., the financial constraint slots remain zero. We set $\dot{b} := h$; the two notations are equivalent and we use h henceforth.

Here $h_{\mathrm{marg}} := (h_1, h_V, h_2)$ denotes the marginal block of h. The perturbed MOT-admissible set is

$$\mathcal{P}^\varepsilon = \big\{\mu \in \Delta(\mathcal{X}) : \mathcal{A}_{\mathrm{marg}}\mu = \mathbf{m} + \varepsilon h_{\mathrm{marg}},\ \mathcal{A}_{\mathrm{fin}}\mu = 0\big\}, \tag{13}$$

and we denote the unique optimizer $\mu^\varepsilon = \arg\inf_{\mu \in \mathcal{P}^\varepsilon} D(\mu\|\bar{\mu})$.

Define the *tangent space of financially-consistent mass-preserving variations*

$$V \ := \ \ker(\mathcal{A}_{\mathrm{fin}}) \cap \ker(\mathbf{1}^\top) \ = \ \big\{v \in \mathbb{R}^{\mathcal{X}} : \mathcal{A}_{\mathrm{fin}} v = 0,\ \textstyle\sum_x v(x) = 0\big\}, \tag{14}$$

and write $W_0 := \{(a_1, a_V, a_2) \in \mathbb{R}^{N_1+N_V+N_2} : \sum a_1 = \sum a_V = \sum a_2 = 0\}$ for the subspace of mass-preserving marginal targets.

Lemma 3.1 (Surjectivity of the reduced constraint map). Under Assumption 2.5, the map $\mathcal{A}_{\mathrm{marg}}|_V : V \to W_0$ is surjective.

Proof. By the finite-dimensional rank theorem it suffices to show the transpose is injective modulo the natural annihilator. Suppose $(y_1, y_V, y_2) \in W_0^\perp$ satisfies $(\mathcal{A}_{\mathrm{marg}}|_V)^\top(y_1, y_V, y_2) = 0$, i.e. $\mathcal{A}_{\mathrm{marg}}^\top(y_1, y_V, y_2) \in V^\perp = \mathrm{range}(\mathcal{A}_{\mathrm{fin}}^\top) + \mathbb{R}\mathbf{1}$. Expanding, there exist $\alpha_{ij}, \beta_{ij} \in \mathbb{R}$ and $c \in \mathbb{R}$ such that for all (i, j, k),

$$y_1(s_1^i) + y_V(v^j) + y_2(s_2^k) \ = \ c + \alpha_{ij}(s_2^k - s_1^i) + \beta_{ij}\big(L(s_2^k/s_1^i) - (v^j)^2\big). \tag{15}$$

Fix (i,j) and vary k. The left-hand side varies only through $y_2(s_2^k)$, so the right-hand side is $\alpha_{ij}s_2^k + \beta_{ij}L(s_2^k/s_1^i) + \text{const}$ as a function of s_2^k. By Assumption 2.5 the functions $\{1,\ s_2 - s_1^i,\ L(s_2/s_1^i) - (v^j)^2\}$ are linearly independent on $\mathcal{S}_2$, so we conclude $\alpha_{ij} = \beta_{ij} = 0$ and y_2 is constant. Substituting back into (15) gives $y_1(s_1^i) + y_V(v^j) = \text{const}$ for all (i,j), which forces y_1 and y_V to be constant as well. The block-sum conditions defining $W_0^\perp$ then force each constant to be zero, so $(y_1, y_V, y_2) = 0$. □

Theorem 3.2 (Well-posedness under marginal perturbations). Suppose $\mu^\star > 0$ and Assumption 2.5 holds. Let (h_1, h_V, h_2) be any mass-preserving marginal perturbation (12). Then there exists $\varepsilon_0 > 0$ such that for all $|\varepsilon| < \varepsilon_0$ the perturbed feasible set $\mathcal{P}^\varepsilon$ (13) is non-empty and the perturbed problem has a unique minimizer μ^ε.

Proof. Since $h_{\text{marg}} = (h_1, h_V, h_2) \in W_0$ (by mass preservation), Lemma 3.1 yields $\dot\mu \in V$ with $\mathcal{A}_{\text{marg}}\dot\mu = h_{\text{marg}}$. Set $\mu(\varepsilon) := \mu^\star + \varepsilon\dot\mu$. By construction, $\mathcal{A}_{\text{marg}}\mu(\varepsilon) = \mathbf{m} + \varepsilon h_{\text{marg}}$, $\mathcal{A}_{\text{fin}}\mu(\varepsilon) = 0$ (since $\dot\mu \in \ker\mathcal{A}_{\text{fin}}$), and $\mathbf{1}^\top\mu(\varepsilon) = 1$. Since $\mu^\star > 0$, there exists $\varepsilon_0 > 0$ such that $\mu(\varepsilon) > 0$ for all $|\varepsilon| < \varepsilon_0$, giving $\mu(\varepsilon) \in \mathcal{P}^\varepsilon$. Uniqueness of the minimizer follows from strict convexity of $D(\cdot\|\bar\mu)$ on the convex set $\mathcal{P}^\varepsilon$. □

3.2 Perturbed Dual Variables And MOT Gibbs Form

By Corollary 2.4, the optimizer μ^ε takes the full MOT Gibbs form. There exist perturbed dual parameters $\theta^\varepsilon = \big(u_1^\varepsilon, u_V^\varepsilon, u_2^\varepsilon, \{\Delta_M^\varepsilon(s_1,v)\}, \{\Delta_C^\varepsilon(s_1,v)\}\big)$ such that

$$\mu^\varepsilon(s_1,v,s_2) \ \propto\ \bar\mu(s_1,v,s_2)\,\exp\Big(u_1^\varepsilon(s_1) + u_V^\varepsilon(v) + u_2^\varepsilon(s_2) + \Delta_M^\varepsilon(s_1,v)(s_2-s_1) + \Delta_C^\varepsilon(s_1,v)\big(L(s_2/s_1) - v^2\big)\Big). \tag{16}$$

At $\varepsilon = 0$ this reduces to the base coupling $\mu^\star$ of (6). It is convenient to collect the dual parameters as

$$\theta^\varepsilon = \theta^\star + \varepsilon\,\dot\theta^0 + o(\varepsilon),$$

where $\theta^\star = (u_1^\star, u_V^\star, u_2^\star, \{\Delta_M^{\star,ij}\}, \{\Delta_C^{\star,ij}\})$ are the base calibrated dual parameters. Working in *scaling variables* $a^\varepsilon(s_1) = e^{u_1^\varepsilon(s_1)}$, $q^\varepsilon(v) = e^{u_V^\varepsilon(v)}$, $c^\varepsilon(s_2) = e^{u_2^\varepsilon(s_2)}$ the Gibbs form becomes

$$\mu^\varepsilon(s_1,v,s_2) \propto \bar\mu(s_1,v,s_2)\,a^\varepsilon(s_1)q^\varepsilon(v)c^\varepsilon(s_2)\,e^{\Delta_M^\varepsilon(s_1,v)(s_2-s_1)+\Delta_C^\varepsilon(s_1,v)(L(s_2/s_1)-v^2)}. \tag{17}$$

Gauge fixing. Only the marginal potentials $(u_1^\varepsilon, u_V^\varepsilon, u_2^\varepsilon)$ carry gauge freedom; the financial multipliers are uniquely determined. We fix

$$\sum_{s_1}\mu_1(s_1)\,u_1^\varepsilon(s_1) = 0, \qquad \sum_{v}\mu_V(v)\,u_V^\varepsilon(v) = 0, \tag{18}$$

pinning down the full parameter vector θ^ε uniquely.

3.3 Differentiability Of The Entropic MOT Projection

We prove that the full MOT optimizer $(\mu^\varepsilon, \theta^\varepsilon)$ depends smoothly on ε and derive the first-order linear system.

The log-partition function $\Lambda(\theta)$ of (5) is C^∞ and strictly convex on the gauge-fixed parameter space (by Proposition 2.6). The full dual objective is

$$\mathcal{D}(\theta;\varepsilon) := \langle \mathbf{m}^\varepsilon,\ \theta_{\text{marg}}\rangle - \Lambda(\theta),$$

where $\mathbf{m}^\varepsilon = (\mu_1^\varepsilon, \mu_V^\varepsilon, \mu_2^\varepsilon)$ and the financial components (Δ_M, Δ_C) enter only through $\Lambda(\theta)$.

Lemma 3.3 (Structural constant-rank of H). Define the null subspace $N := \{v \in \mathbb{R}^K : \langle v, T(x)\rangle = \text{const } \bar\mu\text{-a.e.}\}$. Then $\ker H(\theta) = N$ for every $\theta \in \mathbb{R}^K$, so $\operatorname{rank} H(\theta)$ is constant.

Proof. $H(\theta) = \mathrm{Cov}_{Q_\theta}(T)$ with $Q_\theta \propto \bar{\mu}\, e^{\langle \theta, T\rangle}$. Since $\bar{\mu} > 0$, $Q_\theta \sim \bar{\mu}$ for every θ. Hence $\mathrm{Var}_{Q_\theta}(\langle v, T\rangle) = 0$ iff $\langle v, T(x)\rangle$ is constant Q_θ-a.s., iff it is constant $\bar{\mu}$-a.s., i.e. $v \in N$. □

Theorem 3.4 (Differentiability of MOT optimal parameters and coupling). Fix the gauge (18) and assume $\mu^\star > 0$. Then there exists $\varepsilon_0 > 0$ such that on $(-\varepsilon_0, \varepsilon_0)$:

1. $\varepsilon \mapsto \theta^\varepsilon$ is C^∞,
2. $\varepsilon \mapsto \mu^\varepsilon$ is C^∞ entrywise,
3. the first-order variation $\dot{\theta}^0 := d\theta^\varepsilon/d\varepsilon|_{\varepsilon=0}$ is the unique element of $N^\perp = \mathrm{range}(H)$ solving

$$H\,\dot{\theta}^0 = h, \tag{19}$$

where $H = \nabla^2_\theta \Lambda(\theta^\star)$ is the full MOT Fisher matrix (11), $h = (h_1, h_V, h_2, 0_{N_1 N_V}, 0_{N_1 N_V})$ is the perturbation vector (12), and the minimum-norm solution is $\dot{\theta}^0 = H^+ h$.

Proof. The full KKT optimality conditions for the perturbed dual read

$$\nabla_\theta \Lambda(\theta^\varepsilon) = b^\varepsilon, \tag{20}$$

where $b^\varepsilon = (\mathbf{m}^\varepsilon, 0_{N_1 N_V}, 0_{N_1 N_V})$ stacks the perturbed marginal targets and the (unchanged) financial targets.

By Lemma 3.3, $\ker H(\theta) = N$ is independent of θ, so Λ is invariant under $\theta \mapsto \theta + v$ for any $v \in N$ and descends to a C^∞ strictly convex function $\bar{\Lambda}$ on $N^\perp \cong \mathbb{R}^K/N$. The compression of H to $N^\perp$ is invertible by Proposition 2.6. By Lemma 2.8, $b^\varepsilon - b^0 \in N^\perp$ for small $|\varepsilon|$, so $\nabla\bar{\Lambda}([\theta^\varepsilon]) = [b^\varepsilon]$ is a well-posed equation on $N^\perp$. The classical implicit function theorem applied to this equation on $N^\perp$ yields a unique C^∞ curve $\varepsilon \mapsto \theta^\varepsilon \in N^\perp$. Under Assumption 2.5, $N = \{0\}$ and this reduces to the standard IFT statement.

Differentiating (20) at $\varepsilon = 0$ gives $H\,\dot{\theta}^0 = h$, where $h = db^\varepsilon/d\varepsilon|_{\varepsilon=0}$ is the perturbation vector (12). The minimum-norm solution $\dot{\theta}^0 = H^+ h$ gives the first-order change in *all* dual parameters: marginal potentials *and* financial multipliers simultaneously adjust to maintain the constraints. Differentiability of μ^ε follows from the smooth Gibbs map (16). □

Remark. The financial multiplier components of $\dot{\theta}^0$, namely $\dot{\Delta}^0_M$ and $\dot{\Delta}^0_C$, are determined by the off-diagonal blocks $H_{\mathrm{marg},M}$ and $H_{\mathrm{marg},C}$ of the Fisher matrix. They quantify how the delta and vega hedges must re-adjust to preserve martingality and variance consistency as the SPX/VIX marginals change.

Remark (Lift-independence of the risk formula). The curve $\theta^\varepsilon \in N^\perp$ constructed above is a canonical representative: any other solution of $\nabla_\theta \Lambda(\theta^\varepsilon) = b^\varepsilon$ differs by an element of N. Since $g_G = \mathrm{Cov}_{\mu^\star}(G, T) \in \mathrm{range}(H) = N^\perp$ by Lemma 2.7, the inner product $g_G^\top \theta^\varepsilon$ is independent of the choice of representative and the risk formula $\Pi'(0) = g_G^\top H^+ h$ is unambiguous.

3.4 Risk Representation: Gâteaux Derivative Of Expectations

Let $G : \mathcal{X} \to \mathbb{R}$ be any payoff (bounded is automatic since $\mathcal{X}$ finite). Define the model price under calibration μ^ε by

$$\Pi(\varepsilon) := \mathbb{E}_{\mu^\varepsilon}[G] = \sum_{x \in \mathcal{X}} G(x)\mu^\varepsilon(x).$$

Theorem 3.5 (General risk representation). Let $G : \mathcal{X} \to \mathbb{R}$ be any payoff and let $\Pi(\varepsilon) = \mathbb{E}_{\mu^\varepsilon}[G]$. Under the assumptions of Theorem 3.4, $\varepsilon \mapsto \Pi(\varepsilon)$ is C^1 and

$$\Pi'(0) = \langle h_1, \psi_1\rangle + \langle h_V, \psi_V\rangle + \langle h_2, \psi_2\rangle, \tag{21}$$

where $\psi = (\psi_1, \psi_V, \psi_2)$ are the *marginal influence functions* of G. The full influence vector

$$\Psi := H^+\, g_G \tag{22}$$

has components indexed by all sufficient statistics (4), where $H = \nabla^2_\theta \Lambda(\theta^\star)$ is the full MOT Fisher matrix (11) and

$$(g_G)_k = \mathrm{Cov}_{\mu^\star}(G,\, T_k)$$

runs over $\{T_k\}$ = marginal indicators $\cup$ delta payoffs $\cup$ vega payoffs. The marginal influence functions ψ are the components of Ψ corresponding to the marginal sufficient statistics.

Proof. Since μ^ε is C^1 in ε by Theorem 3.4 and $\mathcal{X}$ is finite, the price

$$\Pi(\varepsilon) = \sum_{x \in \mathcal{X}} G(x)\, \mu^\varepsilon(x)$$

is C^1 and

$$\Pi'(0) = \sum_x G(x)\, \dot{\mu}^0(x),$$

where $\dot{\mu}^0$ denotes $\frac{d}{d\varepsilon}\mu^\varepsilon\big|_{\varepsilon=0}$.

From the full MOT Gibbs representation (16),

$$\mu^\varepsilon(x) = \exp\big(\log \bar{\mu}(x) + \langle \theta^\varepsilon, T(x)\rangle - \Lambda(\theta^\varepsilon)\big),$$

the standard exponential-family differentiation gives

$$\frac{\dot{\mu}^0(x)}{\mu^\star(x)} = \langle \dot{\theta}^0, T(x)\rangle - \mathbb{E}_{\mu^\star}[\langle \dot{\theta}^0, T\rangle],$$

where $T(x)$ is the full sufficient statistic vector (4) and $\dot{\theta}^0 = d\theta^\varepsilon/d\varepsilon|_{\varepsilon=0}$. Substituting into $\Pi'(0) = \sum_x G(x)\dot{\mu}^0(x)$ gives

$$\Pi'(0) = \langle \dot{\theta}^0,\, \mathrm{Cov}_{\mu^\star}(G, T)\rangle = \langle \dot{\theta}^0,\, g_G\rangle, \tag{23}$$

where $(g_G)_k = \mathrm{Cov}_{\mu^\star}(G, T_k)$ over all sufficient statistics.

From Theorem 3.4, $\dot{\theta}^0$ solves $H\,\dot{\theta}^0 = h$ with h as in (12), so $\dot{\theta}^0 = H^+ h$. Substituting into (23),

$$\Pi'(0) = \langle \dot{\theta}^0,\, g_G\rangle = \langle H^+ h,\, g_G\rangle = \langle h,\, H^+ g_G\rangle = \langle h,\, \Psi\rangle,$$

where $\Psi = H^+ g_G$. Since h has non-zero entries only in the marginal block, $\Pi'(0) = \langle h_1, \psi_1\rangle + \langle h_V, \psi_V\rangle + \langle h_2, \psi_2\rangle$ with ψ the marginal components of Ψ.

$$\Pi'(0) = \langle h_1, \psi_1\rangle + \langle h_V, \psi_V\rangle + \langle h_2, \psi_2\rangle.$$

This completes the proof. □

Remark. Equation (21) states: to first order, the price sensitivity of any payoff G under marginal shocks is obtained by pairing the marginal shock directions with a set of influence functions computed from the calibrated Gibbs coupling. This converts "bump-and-revalue" into a mathematically controlled linear response.

3.5 Second-Order Error Bound

The linear response formula derived in Theorem 3.5 is a first-order approximation. The following corollary quantifies its accuracy, establishing that the approximation error is $O(\varepsilon^2)$ in the perturbation size.

Corollary 3.6 (Second-order error bound). Under the assumptions of Theorem 3.4, let $G : \mathcal{X} \to \mathbb{R}$ be any payoff. Then there exists $C < \infty$ such that for all sufficiently small $|\varepsilon|$,

$$\big|\Pi(\varepsilon) - \Pi(0) - \varepsilon\langle h, \psi\rangle\big| \;\le\; C\varepsilon^2\, \|h\|^2. \tag{24}$$

Proof. By Theorem 3.4, $\varepsilon \mapsto \theta^\varepsilon$ is C^1; since Λ is C^∞, the implicit function theorem gives $\varepsilon \mapsto \theta^\varepsilon$ is in fact C^∞, and hence $\varepsilon \mapsto \mu^\varepsilon$ is C^∞ entry-wise. Therefore $\Pi(\varepsilon) = \sum_x G(x)\mu^\varepsilon(x)$ is C^2 in ε, and Taylor's theorem gives

$$\Pi(\varepsilon) = \Pi(0) + \varepsilon\Pi'(0) + \tfrac{1}{2}\varepsilon^2\Pi''(\xi)$$

for some ξ between 0 and ε, with $\Pi'(0) = \langle h, \psi\rangle$ by Theorem 3.5. It remains to show $|\Pi''(\xi)| \le C\|h\|^2$ for a constant C independent of h. From the exponential family differentiation of μ^ε, the second derivative $\ddot{\mu}^\xi$ consists of terms that are either quadratic in $\dot{\theta}^\xi$ or linear in $\ddot{\theta}^\xi$. By Theorem 3.4, $\dot{\theta}^\xi = H^{+,\xi}h$ with $\|h\| = \|(h_1, h_V, h_2, \mathbf{0})\| = \|h\|$, so $\|\dot{\theta}^\xi\| \le \|H^{+,\xi}\|\|h\|$. The second-order term satisfies $\ddot{\theta}^\xi = -(H^\xi)^+\nabla^3\Lambda(\theta^\xi)[\dot{\theta}^\xi, \dot{\theta}^\xi]$, which scales as $\|\dot{\theta}^\xi\|^2$. Hence every term in $\ddot{\mu}^\xi$ is $O(\|h\|^2)$. Since $\mathcal{X}$ is finite and $\mu^\xi > 0$ on the compact interval $|\xi| \le \varepsilon_0$, the operator norms $\|H^{+,\xi}\|$, $\|\nabla^3\Lambda(\theta^\xi)\|$ are bounded uniformly in ξ, giving $|\Pi''(\xi)| = |\sum_x G(x)\ddot{\mu}^\xi(x)| \le C\|h\|^2$ for a constant C depending on $\mu^\star$, $\bar{\mu}$, G but not on h. Substituting into the Taylor remainder completes the proof. □

Remark. The bound (24) confirms that for the small marginal perturbations arising from realistic market bumps, the linear response formula $\Pi(0) + \varepsilon\langle h, \psi\rangle$ is highly accurate: the error is quadratic in both the perturbation size ε and the shock magnitude $\|h\|$.

3.6 Stability Bounds

Proposition 3.7 (Lipschitz stability of potentials and couplings). Under the assumptions of Theorem 3.4, there exists $C > 0$ such that for all sufficiently small ε:

$$\|u^\varepsilon - u^0\| \le C|\varepsilon|\|(h_1, h_V, h_2)\|, \qquad \|\mu^\varepsilon - \mu^\star\|_1 \le C|\varepsilon|\|(h_1, h_V, h_2)\|.$$

Proof. From Theorem 3.4, the full dual variation satisfies $\dot{\theta}^0 = H^+h$ with $\|h\| = \|(h_1, h_V, h_2)\|$. The marginal-potential component $\dot{u}^\varepsilon$ is the projection of $\dot{\theta}^\varepsilon$ onto the marginal block; its norm satisfies $\|\dot{u}^\varepsilon\| \le \|\dot{\theta}^\varepsilon\| \le \|H^{+,\varepsilon}\|\|h\|$. Since H^ε varies continuously in ε and $\mathcal{X}$ is finite, $\|H^{+,\varepsilon}\|$ is bounded by some C on a compact neighborhood. Integrating $\dot{u}^\varepsilon$ over ε yields the first bound. The second bound follows from smoothness of the Gibbs map $\mu^\varepsilon = \mathcal{G}(\theta^\varepsilon)$ and the bounded Jacobian on the same neighborhood. □

3.7 Information-Geometric Interpretation

The perturbation theory admits a precise interpretation in information geometry Amari (2016).

The ambient statistical manifold. Fix the prior $\bar{\mu} > 0$ and the sufficient statistics $\{T_k\}$ of (4). The *statistical manifold* is the full exponential family

$$\mathcal{M} := \left\{ \mu_\theta(x) = \bar{\mu}(x)\,\frac{e^{\langle\theta, T(x)\rangle}}{Z(\theta)} \;:\; \theta \in \mathbb{R}^K \right\}, \tag{25}$$

where $K = N_1 + N_V + N_2 + 2N_1N_V$ and $Z(\theta) = \sum_x \bar{\mu}(x)e^{\langle\theta, T(x)\rangle}$. Every point $\mu_\theta \in \mathcal{M}$ is a valid coupling on $\mathcal{X}$; the calibrated solution $\mu^\star = \mu_{\theta^\star}$ is one specific point on this manifold, determined by the constraint-matching conditions of Corollary 2.4. The parameter space $\mathbb{R}^K$ serves as a global coordinate chart, and the tangent space $T_\theta\mathcal{M}$ at any point is identified with $\mathbb{R}^K$ via the parametrization θ.

The Riemannian metric. By Proposition 2.6, $H(\theta) = \nabla^2_\theta\Lambda(\theta)$ is symmetric positive semi-definite; it serves as the Fisher–Rao metric tensor on $\mathcal{M}$, defining for tangent vectors $u, v \in T_\theta\mathcal{M} \cong \mathbb{R}^K$ the inner product $\langle u, v\rangle_{H(\theta)} := u^\top H(\theta)\, v$. Under Assumption 2.5, $H(\theta) \succ 0$ and the metric is non-degenerate; in general it degenerates on $\ker(H)$. The metric is intrinsic to $\mathcal{M}$; it depends only on the calibrated family, not on any payoff or perturbation.

Direction, functional, and Gâteaux derivative. Two further objects are needed to compute a sensitivity:

- *A tangent direction*: a marginal perturbation $h = (h_1, h_V, h_2, 0, \ldots, 0) \in \mathbb{R}^K$ specifies how the constraint targets change. The linear response system $H\dot{\theta}^0 = h$ resolves h into the corresponding tangent vector $\dot{\theta}^0 = H^+ h$ in $T_{\theta^\star}\mathcal{M}$.
- *A smooth functional*: a payoff $G : \mathcal{X} \to \mathbb{R}$ defines the price map $\Pi : \mathcal{M} \to \mathbb{R}$ by $\Pi(\mu_\theta) := \mathbb{E}_{\mu_\theta}[G]$. Its Euclidean gradient on $\mathcal{M}$ in θ-coordinates is $g_G := \nabla_\theta \Pi(\theta^\star) = \mathrm{Cov}_{\mu^\star}(G, T)$.

The linear response system $H\dot{\theta}^0 = h$ maps the constraint perturbation h to the tangent vector $\dot{\theta}^0 = H^+ h \in T_{\theta^\star}\mathcal{M}$. The Gâteaux derivative of Π at $\mu^\star$ along $\dot{\theta}^0$ is

$$\Pi'(0) \;=\; g_G^\top \dot{\theta}^0 \;=\; g_G^\top H^+ h \;=\; \left\langle H^+ g_G,\, \dot{\theta}^0 \right\rangle_H, \tag{26}$$

where the last equality uses $\langle u, v\rangle_H := u^\top H v$, so that $(H^+ g_G)^\top H \dot{\theta}^0 = g_G^\top \dot{\theta}^0$. The vector $H^+ g_G$ is the *natural gradient* of Π on range(H), its Riemannian gradient with respect to the Fisher metric restricted to range(H). Lemma 2.7 guarantees $g_G \in \mathrm{range}(H)$, so $H^+ g_G$ is well-defined regardless of whether H is invertible. Equation (26) then states that the sensitivity equals the Fisher-metric inner product of the natural gradient with $\dot{\theta}^0$.

This makes the structure explicit: H is fixed at calibration and encodes the local geometry of $\mathcal{M}$; G and h are chosen at risk-generation time and specify which sensitivity is evaluated.

Economic interpretation. The perturbation framework can be interpreted as solving a nearby optimal transport problem whose prior is the calibrated coupling $\mu^\star$. A marginal perturbation corresponds to a change in market forwards or option prices. The entropic projection identifies the closest joint distribution consistent with the new market information.

This perspective shows that the risk sensitivities derived in this paper are not tied to any specific stochastic volatility model. Instead they arise from the geometry of the calibrated transport plan. In this sense the risk generation mechanism is largely model independent.

4 Financial Perturbations: Spot And Volatility Bumps

This section translates two standard market perturbations (an SPX spot bump and a parallel SPX implied volatility bump) into admissible perturbation vectors $h = (h_1, h_V, h_2, \mathbf{0})$ in the sense of Section 3.

The SPX components h_1 and h_2 are derived here directly from the perturbed marginals. The VIX component h_V is *not* zero: an SPX perturbation changes the SPX forward variance, which shifts the VIX future level F_V through the forward-variance replication identity, and this shift already induces a change in the VIX marginal μ_V before any smile dynamics are imposed. The SSR rule of Section 5.4 then further propagates this shift to the full VIX implied volatility surface. We therefore leave h_V as a *placeholder* in this section, to be completed in Section 5.4.

4.1 SPX Spot Perturbation

Setup. Under a sticky-strike convention, shifting the spot $S_0 \mapsto S_0 + \delta_S$ translates the SPX forward distribution at both maturities T_1 and T_2 by δ_S (exact under flat-smile/Bachelier dynamics; a first-order approximation in general). On the discrete grids $\mathcal{S}_j = \{s_j^i\}_{i=1}^{N_j}$, $j \in \{1, 2\}$, define

$$\mu_j^{\delta_S}(s_j^i) \;:=\; \mu_j(s_j^i - \delta_S), \tag{27}$$

where $\mu_j(\cdot)$ is extended off-grid by piecewise-linear interpolation.

Assumption 4.1 (Interior support). The grids $\mathcal{S}_1$ and $\mathcal{S}_2$ are padded so that $\mu_j(s_j^1) = \mu_j(s_j^{N_j}) = 0$ for $j \in \{1, 2\}$, i.e., the support of each marginal is strictly interior to the grid.

Remark. Translation invariance of a Lebesgue integral, $\int f(x - \delta_S)\, dx = \int f(x)\, dx$, does *not* transfer to a finite discrete sum on a truncated grid: $\sum_i \mu_j(s_j^i - \delta_S)$ loses mass at the boundary unless Assumption 4.1 holds. In practice, the grids used in calibration extend well beyond the range of quoted strikes, so boundary masses are negligible; Assumption 4.1 formalises this.

Proposition 4.2 (Spot bump defines an admissible perturbation). Under Assumption 4.1, for $|\delta_S| < h_{\text{grid}} := \min_i(s_j^{i+1} - s_j^i)$, $\mu_j^{\delta_S}$ is a valid probability measure on $\mathcal{S}_j$ for $j \in \{1, 2\}$, and the directional derivatives

$$h_j(s_j^i) \;:=\; \frac{d}{d\delta_S}\mu_j^{\delta_S}(s_j^i)\Big|_{\delta_S=0} \;=\; -\mu_j'(s_j^i) \tag{28}$$

satisfy $\sum_i h_j(s_j^i) = 0$.

Proof. By piecewise-linear interpolation with mesh spacing h_{grid}, for $\delta_S \in (0, h_{\text{grid}})$,

$$\mu_j^{\delta_S}(s_j^i) \;=\; \big(1 - \tfrac{\delta_S}{h_{\text{grid}}}\big)\mu_j(s_j^i) + \tfrac{\delta_S}{h_{\text{grid}}}\mu_j(s_j^{i-1}),$$

where $\mu_j(s_j^0) := 0$ by convention. Summing over $i = 1, \ldots, N_j$ and using Assumption 4.1 ($\mu_j(s_j^1) = \mu_j(s_j^{N_j}) = 0$):

$$\sum_i \mu_j^{\delta_S}(s_j^i) \;=\; \big(1 - \tfrac{\delta_S}{h_{\text{grid}}}\big)\sum_i \mu_j(s_j^i) + \tfrac{\delta_S}{h_{\text{grid}}}\sum_i \mu_j(s_j^{i-1}) \;=\; 1,$$

where the last equality holds because both inner sums equal 1 (the boundary-zero assumption prevents mass leaving the grid). Positivity for small $|\delta_S|$ follows from linear interpolation. Differentiating (27) at $\delta_S = 0$ gives $h_j = -\mu_j'$ (28), and $\sum_i h_j(s_j^i) = d/d\delta_S\big[\sum_i \mu_j^{\delta_S}(s_j^i)\big]_{\delta_S=0} = 0$. □

Remark. An equivalent construction that bypasses Assumption 4.1 is the *barycentric pushforward*: each atom at s_j^i is mapped to $s_j^i + \delta_S$, then redistributed linearly between the two nearest grid points (with mass reaching outside the grid absorbed at the boundary). This defines a stochastic matrix P_{δ_S} and sets $\mu_j^{\delta_S} := P_{\delta_S}\mu_j$; mass is preserved exactly for all δ_S, and the resulting h_j agrees with $-\mu_j'$ to first order.

Perturbation vector. For the spot bump, the perturbation vector is

$$h^{\text{spot}} \;=\; \Big(-\mu_1'(\cdot),\; \underbrace{h_V}_{\text{see Sec. 5.4}},\; -\mu_2'(\cdot),\; \underbrace{0, \ldots, 0}_{\text{financial slots}}\Big) \;\in\; \mathbb{R}^K, \tag{29}$$

where $-\mu_j'$ denotes the discrete derivative of the marginal μ_j (28). The VIX component h_V is non-zero because the spot bump shifts the SPX forward variance and hence the VIX future F_V; its explicit form is derived in Section 5.4.

4.2 SPX Implied Volatility Perturbation

Setup. A parallel implied volatility bump applied to both SPX maturities shifts

$$\sigma(K, T_i) \;\mapsto\; \sigma(K, T_i) + \delta_\sigma, \qquad i \in \{1, 2\}.$$

At each maturity T_i, the perturbed call prices follow from Black-Scholes Black and Scholes (1973),

$$C_i^{\delta_\sigma}(K) \;:=\; C_{BS}\big(S_0, K, T_i,\, \sigma(K, T_i) + \delta_\sigma\big), \tag{30}$$

and Breeden-Litzenberger inversion Breeden and Litzenberger (1978) yields the perturbed marginal density:

$$\mu_i^{\delta_\sigma}(s) \;=\; \frac{\partial^2 C_i^{\delta_\sigma}}{\partial K^2}\Big|_{K=s}, \qquad i \in \{1, 2\}. \tag{31}$$

Assumption 4.3 (Strict positivity of base marginals on the grid). The calibrated base marginals satisfy $\mu_i(s) > 0$ for every grid point $s \in \mathcal{S}_i$, $i \in \{1, 2\}$.

Remark. Assumption 4.3 is a consequence of the strictly positive feasible coupling (A3) of Theorem 2.3: if $\mu_0 \in \mathcal{P}$ with $\mu_0(s_1, v, s_2) > 0$ everywhere, then each marginal $\mu_i(s) = \sum_{(s_1,v,s_2):s_i=s} \mu_0(s_1, v, s_2) > 0$. Economically, it states that the calibrated model assigns positive probability to every grid state, a property satisfied by any Gibbs coupling with a strictly positive prior $\bar{\mu} > 0$.

Proposition 4.4 (Volatility bump defines admissible perturbations). For sufficiently small $|\delta_\sigma|$, $\mu_i^{\delta_\sigma}$ is a valid probability measure on $\mathcal{S}_i$ for each $i \in \{1, 2\}$, and the directional derivatives

$$h_i(s) \;:=\; \frac{d}{d\delta_\sigma}\mu_i^{\delta_\sigma}(s)\Big|_{\delta_\sigma=0} \;=\; \frac{\partial^2 \mathsf{V}^{BS}_{\mathrm{SPX},i}}{\partial K^2}\Big|_{K=s}, \tag{32}$$

where $\mathsf{V}^{BS}_{\mathrm{SPX},i}(K) := \partial_\sigma C_{BS}(S_0, K, T_i, \sigma(K, T_i))$ is the Black-Scholes vega at maturity T_i and strike K, each satisfy $\sum_s h_i(s) = 0$.

Proof. Since C_{BS} is C^∞ in σ, the map $\delta_\sigma \mapsto C_i^{\delta_\sigma}(K)$ is C^∞ jointly in (K, δ_σ). The Breeden-Litzenberger density therefore expands as

$$\mu_i^{\delta_\sigma}(s) \;=\; \mu_i(s) + \delta_\sigma\, h_i(s) + O(\delta_\sigma^2), \tag{33}$$

where $h_i(s) = \partial_K^2 \mathsf{V}^{BS}_{\mathrm{SPX},i}|_{K=s}$ as in (32). The naive implication $\sigma + \delta_\sigma > 0 \Rightarrow \partial_K^2 C^{\delta_\sigma} \geq 0$ fails on a skewed smile (the Breeden-Litzenberger formula involves $\sigma'(K)$ and $\sigma''(K)$, so density positivity is not implied merely by vol positivity). The correct argument is quantitative and discrete. By Assumption 4.3, the base marginal is strictly positive on the finite grid $\mathcal{S}_i$, so

$$\underline{\mu}_i \;:=\; \min_{s\in\mathcal{S}_i} \mu_i(s) \;>\; 0, \qquad \overline{h}_i \;:=\; \max_{s\in\mathcal{S}_i} |h_i(s)| \;<\; \infty.$$

Setting $\bar{\delta}_{\sigma,i} := \underline{\mu}_i/(2\overline{h}_i)$, uniform continuity of the $O(\delta_\sigma^2)$ remainder on the finite grid gives a constant C_i such that for $|\delta_\sigma| \leq \bar{\delta}_{\sigma,i}$:

$$\mu_i^{\delta_\sigma}(s) \;\geq\; \underline{\mu}_i - |\delta_\sigma|\,\overline{h}_i - C_i\delta_\sigma^2 \;\geq\; \tfrac{1}{2}\underline{\mu}_i \;>\; 0.$$

Additionally $|\delta_\sigma| < \min_K \sigma(K, T_i)$ ensures $\sigma(K, T_i) + \delta_\sigma > 0$ (implied vols remain positive), so $C_i^{\delta_\sigma}$ is a valid Black-Scholes price. The admissible range is $|\delta_\sigma| \leq \min\{\bar{\delta}_{\sigma,i}, \min_K \sigma(K, T_i)\}$.

Mass preservation follows from the boundary conditions $C_i^{\delta_\sigma}(0) = S_0$ and $C_i^{\delta_\sigma}(K) \to 0$ as $K \to \infty$, which hold for all δ_σ. Differentiating (31) with respect to δ_σ at $\delta_\sigma = 0$ and exchanging $d/d\delta_\sigma$ with ∂_K^2 (justified by smoothness):

$$h_i(s) = \frac{\partial^2}{\partial K^2}\underbrace{\frac{dC_i^{\delta_\sigma}}{d\delta_\sigma}\Big|_{\delta_\sigma=0}}_{\mathsf{V}^{BS}_{\mathrm{SPX},i}(K)}\Big|_{K=s} = \frac{\partial^2 \mathsf{V}^{BS}_{\mathrm{SPX},i}}{\partial K^2}\Big|_{K=s},$$

establishing (32). The mass-zero conditions follow by differentiating $\sum_s \mu_i^{\delta_\sigma}(s) = 1$ with respect to δ_σ at $\delta_\sigma = 0$, as in Proposition 4.2. □

Perturbation vector. For the parallel vol bump, the perturbation vector is

$$h^{\mathrm{vol}} \;=\; \Big(\partial_K^2 \mathsf{V}^{BS}_{\mathrm{SPX},T_1}\big|_{K=\cdot},\; \underbrace{h_V}_{\text{see Sec. 5.4}},\; \partial_K^2 \mathsf{V}^{BS}_{\mathrm{SPX},T_2}\big|_{K=\cdot},\; \underbrace{0, \ldots, 0}_{\text{financial slots}}\Big) \;\in\; \mathbb{R}^K, \tag{34}$$

where $\mathsf{V}^{BS}_{\mathrm{SPX},T_i}(K) = \partial_\sigma C_{BS}(S_0, K, T_i, \sigma(K, T_i))$ is the Black-Scholes vega at maturity T_i (32). If instead a single-maturity bump is applied (e.g. only T_1), then the $\partial_K^2 \mathsf{V}^{BS}_{\mathrm{SPX},T_2}$ component is zero. In both cases $h_V \neq 0$ and is completed in Section 5.4.

Summary. In both cases the perturbation vector h is admissible in the sense of Section 3: each non-zero component is mass-preserving and the financial constraint slots are zero. The risk sensitivity for any payoff G is then $\Pi'(0) = g_G^\top H^+ h$, with h assembled from (29) or (34) respectively. The LR method enforces all three components (h_1, h_V, h_2) simultaneously through the Fisher linear system; the treatment of h_2 under the DR method is discussed in Remark 7.2 once that framework has been introduced (Section 7).

5 SSR Dynamics For VIX And Its Linearization

5.1 Skew Stickiness Ratio: Bergomi's Definition And Extension To VIX

We now give a formal definition of the Skew Stickiness Ratio (SSR) following Bergomi (2016, 2009). Let $\sigma(K, F)$ denote the implied volatility of an option with strike K and forward level F of the underlying asset. Bergomi models smile dynamics by expressing first-order reactions of the volatility surface to changes in the forward.

5.1.1 Bergomi's Definition of Skew Stickiness Ratio

Following Bergomi (2016, 2009), let $\sigma^*(F) := \sigma(F, F)$ denote the at-the-money-forward (ATMF) implied volatility and let

$$S_{\log}(F) := \left.\frac{\partial \sigma}{\partial \ln K}\right|_{K=F} = F \left.\frac{\partial \sigma(K,F)}{\partial K}\right|_{K=F} \tag{35}$$

be the *ATM log-moneyness skew*. For equity underlyings the leverage effect drives $S_{\log} < 0$.

Bergomi's Skew Stickiness Ratio β (SSR) is the dimensionless parameter defined through the floating-ATMF sensitivity

$$\frac{d\sigma^*(F)}{d\ln F} = \beta \cdot S_{\log}(F). \tag{36}$$

Equivalently, the sensitivity of fixed-strike vol at $K = F$ is

$$\left.\frac{\partial \sigma(K,F)}{\partial F}\right|_{K=F} = (\beta - 1)\,\frac{S_{\log}(F)}{F} = (\beta - 1) \left.\frac{\partial \sigma}{\partial K}\right|_{K=F}, \tag{37}$$

and for a general strike K the self-similar (SSR) surface satisfies

$$\left.\frac{\partial \sigma(K,F)}{\partial F}\right|_{K \text{ fixed}} = (\beta - 1)\,\frac{K}{F} \left.\frac{\partial \sigma}{\partial K}\right|_{K}. \tag{38}$$

Thus a perturbation δF in the forward produces the leading-order smile shift

$$\delta\sigma(K) = (\beta - 1)\,\frac{K}{F}\,\partial_K \sigma(K)\,\delta F \qquad (K \text{ fixed}), \tag{39}$$

or, using the ATM uniform approximation, $\delta\sigma \approx (\beta - 1)\, S_{\log}(F)\, \delta F / F$.

The stickiness regimes are:

- $\beta = 0$: Sticky delta (smile frozen in K/F; $d\sigma^*/d\ln F = 0$),
- $\beta = 1$: Sticky strike (fixed-K vol frozen; $\partial_F \sigma|_K = 0$),
- $\beta \approx \frac{3}{2}$: Empirical SPX value Bergomi (2016),
- $\beta > 1$: Super-skew (fixed-K vol moves *opposite* to F, amplifying the leverage effect beyond sticky-strike).

Remark (Sign convention for equity). For equity indices $S_{\log} < 0$ and $\beta > 0$, so $d\sigma^*/d\ln F = \beta S_{\log} < 0$: the floating ATMF vol rises when the spot falls. For $\beta > 1$ the fixed-K vol also falls when the spot rises ($\partial_F \sigma|_{K=F} = (\beta - 1) S_{\log}/F < 0$), consistent with the leverage effect. At $\beta = 1$ (sticky-strike) the fixed-K vol is unchanged, and the entire ATMF rise comes from the smile sliding along the strike axis.

5.1.2 Extension to VIX Futures And VIX Options

Let F_V denote the VIX future level, $\sigma_V(K, F_V)$ the VIX option implied volatility, and $\sigma_V^*(F_V) := \sigma_V(F_V, F_V)$ the ATMF VIX vol. Define the VIX ATM log-moneyness skew

$$S_{\log,V}(F_V) := F_V \left.\frac{\partial \sigma_V(K, F_V)}{\partial K}\right|_{K=F_V}.$$

VIX options have a positively-sloped smile, so $S_{\log,V} > 0$.

The VIX Skew Stickiness Ratio β_V is defined by the same floating-ATMF condition as (36):

$$\frac{d\sigma_V^*(F_V)}{d\ln F_V} = \beta_V \cdot S_{\log,V}(F_V). \tag{40}$$

The corresponding fixed-strike sensitivity for general K is

$$\left.\frac{\partial \sigma_V(K, F_V)}{\partial F_V}\right|_{K \text{ fixed}} = (\beta_V - 1)\,\frac{K}{F_V}\,\partial_K \sigma_V(K), \qquad \beta_V > 0. \tag{41}$$

At the ATM point $K = F_V$ this reduces to

$$\left.\frac{\partial \sigma_V(K, F_V)}{\partial F_V}\right|_{K=F_V} = (\beta_V - 1)\,\frac{S_{\log,V}}{F_V} = (\beta_V - 1)\left.\frac{\partial \sigma_V}{\partial K}\right|_{K=F_V}. \tag{42}$$

The corresponding linearized vol shift for a finite move δF_V is

$$\delta\sigma_V(K) = (\beta_V - 1)\,\frac{K}{F_V}\,\partial_K \sigma_V(K)\,\delta F_V \qquad (K \text{ fixed}). \tag{43}$$

Remark (Sign convention for VIX). Since $S_{\log,V} > 0$ and empirically $\beta_V \approx 1.2 > 1$, we have $(\beta_V - 1) > 0$: when VIX rises ($\delta F_V > 0$) the fixed-K VIX vol also rises ($\delta\sigma_V > 0$), consistent with market observation. At $\beta_V = 1$ (sticky-strike) the VIX vol surface would be frozen in absolute strike space.

5.2 Linear SSR Approximation And Second–Order Accuracy

Using the SSR definition (40) and the fixed-strike identity (41), we now formalise the linearisation with a quantitative second-order error bound.

Theorem 5.1 (Unified linear SSR expansion with second-order error). Assume $\sigma_V(K, F_V)$ is C^2 in F_V near the base level. Let $F_V' = F_V + \delta F_V$. Then the implied volatility satisfies

$$\sigma_V(K, F_V') = \sigma_V(K, F_V) + (\beta_V - 1)\,\frac{K}{F_V}\,\partial_K \sigma_V(K)\,\delta F_V + R_K(\delta F_V), \tag{44}$$

where the remainder satisfies the deterministic bound

$$\left|R_K(\delta F_V)\right| \le \frac{1}{2} \sup_{|u - F_V| \le |\delta F_V|} \left|\frac{\partial^2 \sigma_V(K, u)}{\partial F_V^2}\right| (\delta F_V)^2. \tag{45}$$

In particular, the *strike-dependent linear SSR approximation*

$$\sigma_V(K, F_V') \approx \sigma_V(K, F_V) + (\beta_V - 1)\,\frac{K}{F_V}\,\partial_K \sigma_V(K)\,(F_V' - F_V) \tag{46}$$

is first-order accurate with $O((\delta F_V)^2)$ error controlled by (45). The *uniform (ATM) approximation* replaces $\frac{K}{F_V}\partial_K \sigma_V(K)$ by its ATM value $S_{\log,V}/F_V$:

$$\sigma_V(K, F_V') \approx \sigma_V(K, F_V) + (\beta_V - 1)\,\frac{S_{\log,V}}{F_V}\,(F_V' - F_V). \tag{47}$$

Proof. Apply Taylor's theorem in F_V:

$$\sigma_V(K, F_V + \delta F_V) = \sigma_V(K, F_V) + \frac{\partial \sigma_V}{\partial F_V}(K, F_V)\,\delta F_V + \frac{1}{2}\,\frac{\partial^2 \sigma_V}{\partial F_V^2}(K, \xi)\,(\delta F_V)^2,$$

for some ξ between F_V and $F_V + \delta F_V$. Substituting the SSR identity (38)

$$\frac{\partial \sigma_V}{\partial F_V}(K, F_V) = (\beta_V - 1)\,\frac{K}{F_V}\,\partial_K \sigma_V(K)$$

into the first-order term gives (44), and the bound (45) follows by taking the supremum over the interval. □

Interpretation. The first-order term in (44) gives the SSR-based linear smile reaction used in the perturbed optimal transport constraints. The explicit $O(\delta^2)$ bound in (45) quantifies the approximation error and shows that the SSR mapping is highly accurate for the small forward perturbations relevant for risk generation.

5.3 Empirical Evidence For VIX Skew Stickiness Ratio

Skew Stickiness Ratio (SSR) is widely used by practitioners to describe how the VIX volatility smile responds to changes in the underlying SPX level.

To estimate SSR empirically we regress daily changes in VIX implied volatility against changes in the VIX future level across different maturities. Figure 1 illustrates the estimated SSR term structure using historical windows from six months to three years.

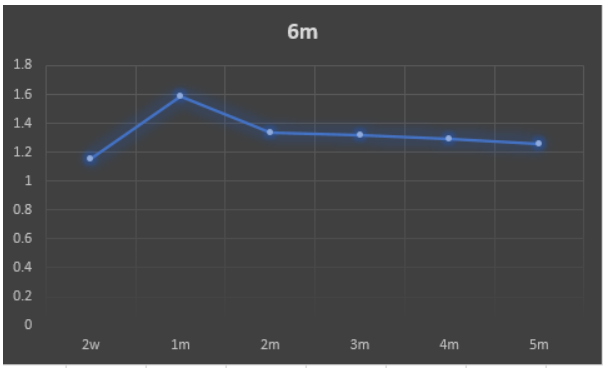

(a) 6m window

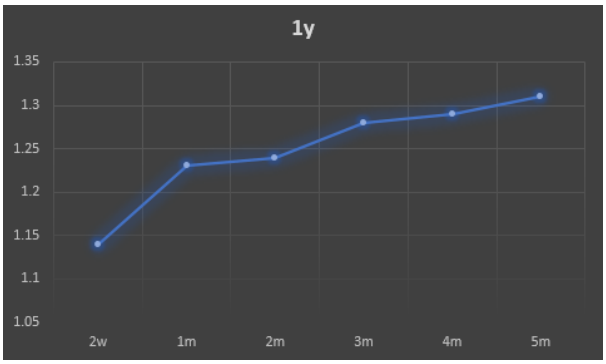

(b) 1y window

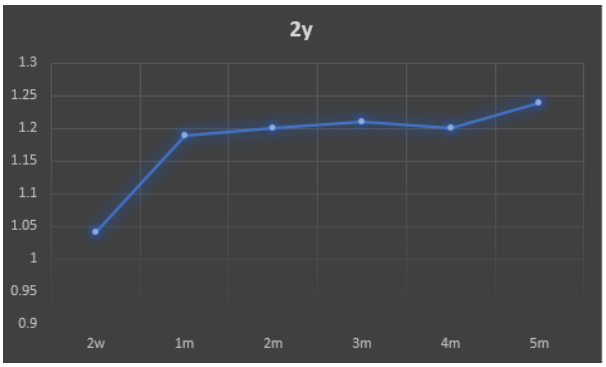

(c) 2y window

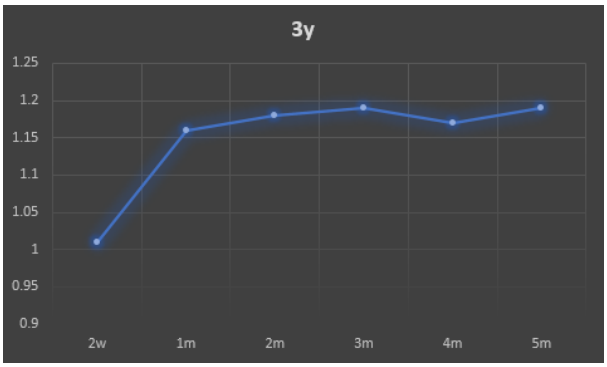

(d) 3y window

Figure 1: Estimated VIX SSR term structure across four historical windows.

These estimates confirm $\beta_V \approx 1.2$ used in the numerical experiments.

5.4 Completing h_V: SSR Propagation To The VIX Marginal

We now complete the perturbation vector left open in Section 4 by deriving the VIX marginal component h_V. The argument has four steps: (1) compute the forward-variance shift $\delta\sigma^2_{\text{fwd}}$ from the SPX marginal perturbation; (2) apply the linearized SSR rule to define the sensitivity kernel $\Gamma(K)$ and the shape vector A_{SSR}; (3) determine δF_V exactly from the variance-consistency constraint; (4) invert via Breeden–Litzenberger to obtain h_V.

Step 1: Forward-variance shift from the SPX marginals. The SPX-implied forward variance is the expected log-contract:

$$\sigma^2_{\text{fwd}} \;=\; \mathbb{E}_{\mu^\star}[L(S_2/S_1)].$$

Since $L(S_2/S_1) = L(S_2) - L(S_1)$ (both $L(s) = -\frac{2}{\tau}\ln s$ applied to absolute levels), the expectation separates into marginals:

$$\sigma^2_{\text{fwd}} \;=\; \mathbb{E}_{\mu_2}[L(\cdot)] - \mathbb{E}_{\mu_1}[L(\cdot)] \;=\; \sum_{s_2\in\mathcal{S}_2} L(s_2)\,\mu_2(s_2) \;-\; \sum_{s_1\in\mathcal{S}_1} L(s_1)\,\mu_1(s_1).$$

Under the SPX marginal perturbation (h_1, h_2), the first-order change in forward variance is

$$\delta\sigma^2_{\text{fwd}} \;=\; \langle L,\, h_2\rangle_{\mathcal{S}_2} \;-\; \langle L,\, h_1\rangle_{\mathcal{S}_1}, \tag{48}$$

where $\langle L, h_i\rangle_{\mathcal{S}_i} = \sum_{s\in\mathcal{S}_i} L(s)\,h_i(s)$. This is exact (by linearity of expectation) and depends only on the SPX marginal components h_1, h_2.

Step 2: SSR sensitivity kernel. Applying the SSR rule (43), the first-order change in VIX implied volatility is $\delta\sigma_V(K)$ as defined there. The corresponding change in VIX call prices via Black's formula is:

$$\delta C_V(K) \;=\; \underbrace{\Big[\Delta^{BS}_V(K) + (\beta_V - 1)\,\frac{K}{F_V}\,\partial_K\sigma_V(K)\,\mathsf{V}^{BS}_{\text{VIX}}(K)\Big]}_{\Gamma(K)}\,\delta F_V, \tag{49}$$

where $\Delta^{BS}_V(K) = \partial_{F_V} C_V(K)$ is the VIX option delta, $\mathsf{V}^{BS}_{\text{VIX}}(K) = \partial_{\sigma_V} C_V(K)$ is the VIX option vega, and $\Gamma(K)$ is the combined sensitivity kernel. Applying Breeden-Litzenberger Breeden and Litzenberger (1978) to (49) gives the shape vector

$$A_{\text{SSR}}(v) \;:=\; \frac{\partial^2\Gamma}{\partial K^2}\Big|_{K=v}, \tag{50}$$

where $v \in \mathcal{V}$ denotes a generic VIX grid point, so that $h_V = A_{\text{SSR}}\,\delta F_V$ once δF_V is known.

Lemma 5.2 (Positivity of the SSR denominator). Assume:

(B1) *(Boundary decay)* The VIX call surface satisfies $(K - F_V)^2|\Gamma'(K)| \to 0$ as $K \to 0^+$ and $K \to \infty$.

(B2) *(Non-negative kernel)* $\Gamma(K) \geq 0$ for all $K > 0$.

Then $\langle v^2, A_{\text{SSR}}\rangle > 0$.

Proof. Integrate by parts twice with $u = K^2$ and $dv = \Gamma''(K)\,dK$:

$$\int_0^\infty K^2\,\Gamma''(K)\,dK \;=\; \big[K^2\Gamma'(K)\big]_0^\infty - 2\big[K\Gamma(K)\big]_0^\infty + 2\int_0^\infty \Gamma(K)\,dK.$$

Both boundary terms vanish. The first, $[K^2\Gamma'(K)]_0^\infty$, vanishes by (B1): since $K^2/(K-F_V)^2 \to 1$ as $K \to \infty$ and $K^2/F_V^2 \to 0$ as $K \to 0^+$, (B1) implies $K^2|\Gamma'(K)| \to 0$ at both endpoints. The second, $[2K\Gamma(K)]_0^\infty$, vanishes trivially at $K \to 0^+$ (since $K \to 0$ with $\Gamma(0)$ finite) and exponentially at $K \to \infty$ (since $\Gamma(K) \le \Delta_V^{BS}(K)$ decays faster than any polynomial). Hence

$$\langle v^2, A_{\mathrm{SSR}} \rangle \;=\; 2\int_0^\infty \Gamma(K)\, dK.$$

Under (B2), $\Gamma \ge 0$ on $(0,\infty)$. Since $\Gamma(0) = \Delta_V^{BS}(0) = 1 > 0$ and Γ is continuous, $\int_0^\infty \Gamma(K)\, dK > 0$, so $\langle v^2, A_{\mathrm{SSR}} \rangle > 0$. □

Remark (When (B2) holds). Both terms of $\Gamma(K) = \Delta_V^{BS}(K) + (\beta_V - 1)\frac{K}{F_V}\partial_K \sigma_V(K)\mathsf{V}_{\mathrm{VIX}}^{BS}(K)$ are non-negative when $\beta_V \ge 1$ and the VIX skew is non-negative ($\partial_K \sigma_V \ge 0$), which is the empirically observed regime for VIX ($\beta_V \approx 1.2$, positive skew). At $\beta_V = 1$ (sticky-strike), $\Gamma = \Delta_V^{BS} > 0$ always. For $\beta_V < 1$, (B2) requires that the delta term dominates the (now negative) vega contribution, which holds whenever $|1-\beta_V|$ is not too large relative to the skew level.

Step 3: Variance-anchored determination of δF_V. The MOT variance-consistency condition $\mathbb{E}_{\mu^\star}[V^2] = \sigma_{\mathrm{fwd}}^2$ links the second moment of μ_V to the forward variance. Differentiating the exact identity $\sigma_{\mathrm{fwd}}^2 = F_V^2 + \mathrm{Var}_{\mu_V}(V)$ and substituting $h_V = A_{\mathrm{SSR}}\,\delta F_V$:

$$\begin{aligned}
\delta\sigma_{\mathrm{fwd}}^2 \;&=\; 2F_V\,\delta F_V + \delta\mathrm{Var}_{\mu_V}(V) \\
&=\; 2F_V\,\delta F_V + \big(\langle v^2, A_{\mathrm{SSR}}\rangle - 2F_V\big)\delta F_V \\
&=\; \langle v^2,\, A_{\mathrm{SSR}}\rangle\,\delta F_V,
\end{aligned}$$

where the second line uses $\delta\mathrm{Var}_{\mu_V}(V) = \langle v^2, h_V\rangle - 2F_V\,\delta F_V = \langle v^2, A_{\mathrm{SSR}}\rangle\,\delta F_V - 2F_V\,\delta F_V$. By Lemma 5.2 (under (B1)–(B2)), the denominator $\langle v^2, A_{\mathrm{SSR}}\rangle > 0$, so solving gives the exact, non-circular formula:

$$\delta F_V \;=\; \frac{\delta\sigma_{\mathrm{fwd}}^2}{\langle v^2,\, A_{\mathrm{SSR}}\rangle_{\mathcal{V}}}. \tag{51}$$

Step 4: Breeden–Litzenberger inversion. With δF_V determined by (51), the VIX marginal perturbation is:

$$h_V(v) \;=\; A_{\mathrm{SSR}}(v)\,\delta F_V \;=\; \frac{\partial^2\Gamma}{\partial K^2}\bigg|_{K=v} \cdot \frac{\delta\sigma_{\mathrm{fwd}}^2}{\langle v^2,\, A_{\mathrm{SSR}}\rangle}, \tag{52}$$

where A_{SSR} and $\Gamma(K)$ are defined in (50) and (49). The mass-zero condition $\sum_v h_V(v) = 0$ follows because $\langle 1, A_{\mathrm{SSR}}\rangle = 0$. By the fundamental theorem of calculus, $\int_0^\infty \Gamma''(K)\, dK = \big[\Gamma'(K)\big]_0^\infty$, where $\Gamma'(K) = -\partial_{F_V} P(V > K)$ is the derivative of the (negated) VIX risk-neutral survival function with respect to F_V. At $K \to 0^+$, $P(V > 0) = 1$ identically (VIX is strictly positive), so $\Gamma'(0^+) = 0$; at $K \to \infty$, $P(V > K) \to 0$ identically, so $\Gamma'(\infty) = 0$. Hence $\langle 1, A_{\mathrm{SSR}}\rangle = 0 - 0 = 0$.

Complete perturbation vector. Assembling all three components, the full admissible perturbation vector is

$$h \;=\; \big(h_1,\; h_V,\; h_2,\; \underbrace{0, \ldots, 0}_{\text{financial slots}}\big) \;\in\; \mathbb{R}^K, \tag{53}$$

where h_1, h_2 are given by Section 4, h_V by (52), and the financial slots remain zero since the martingale and variance-consistency constraints are structural. The risk sensitivity of any payoff G under the fully propagated SPX perturbation is then

$$\Pi'(0) \;=\; g_G^\top H^+ h,$$

with h from (53).

6 Algorithm For SPX–VIX Risk Without Recalibration

6.1 Base Calibration

We first compute a base joint coupling between the SPX state S_1, the VIX variable V, and the future SPX state S_2. The goal of this calibration step is to construct a probability measure

$$\mu(s_1, v, s_2)$$

that matches the prescribed SPX and VIX marginals while simultaneously enforcing the key financial consistency conditions linking SPX and VIX dynamics.

Specifically, the calibrated coupling must satisfy:

- the marginal constraints

$$(\mathcal{A}_{\text{marg}}\mu)_1 = \mu_1, \qquad (\mathcal{A}_{\text{marg}}\mu)_V = \mu_V, \qquad (\mathcal{A}_{\text{marg}}\mu)_2 = \mu_2,$$

  corresponding to the SPX spot, VIX, and future SPX marginals implied by market prices;

- the financial constraints $\mathcal{A}_{\text{fin}}\mu = 0$, i.e. the martingale and variance-consistency conditions defined in Section 2.

Numerically, we solve this constrained calibration problem using a nested scheme. An outer Sinkhorn iteration enforces the marginal constraints via multiplicative scaling factors, while an inner Newton (or damped Newton) correction enforces the conditional martingale and variance-consistency conditions at each (S_1, V) node.

This structure closely follows the constrained calibration framework introduced in the SPX–VIX joint calibration methodology of Guyon (2020), where optimal transport techniques are combined with financial consistency constraints to produce arbitrage-consistent joint distributions.

The resulting calibrated coupling $\mu^\star$ serves as the base distribution for the subsequent perturbation and risk-generation procedures described in the following sections.

Algorithm 1: Base Calibration Via Sinkhorn With Newton/LM Enforcement

1. **Inputs.** Discrete grids $\mathcal{S}_1, \mathcal{V}, \mathcal{S}_2$; target marginals μ_1, μ_V, μ_2; prior $\bar{\mu}(s_1, v, s_2)$; log-return functional $L(\cdot)$; marginal tolerance $\varepsilon_{\text{marg}}$; financial tolerance ε_{fin}; Newton damping $\lambda \geq 0$.

2. **Outputs.** Calibrated coupling $\mu^\star(s_1, v, s_2)$ and Fisher information matrix H.

3. **Initialize.**

$$a(s_1) \leftarrow 1, \quad q(v) \leftarrow 1, \quad c(s_2) \leftarrow 1, \qquad \Delta_M(s_1, v) \leftarrow 0, \quad \Delta_C(s_1, v) \leftarrow 0.$$

   Form initial Gibbs coupling

$$\mu(s_1, v, s_2) \propto \bar{\mu}(s_1, v, s_2)\, a(s_1) q(v) c(s_2) \exp\{\Delta_M(s_1, v)(s_2 - s_1) + \Delta_C(s_1, v)(L(s_2/s_1) - v^2)\}.$$

4. **Outer loop:** repeat until marginal errors $\leq \varepsilon_{\text{marg}}$ and financial residuals $\leq \varepsilon_{\text{fin}}$:

   (a) **Sinkhorn marginal updates:** for all grid points update

$$a(s_1) \leftarrow \frac{\mu_1(s_1)}{\sum_{v, s_2} \bar{\mu}(s_1, v, s_2)\, q(v) c(s_2)\, e^{\Delta_M(s_1, v)(s_2 - s_1) + \Delta_C(s_1, v)(L(s_2/s_1) - v^2)}},$$

$$q(v) \leftarrow \frac{\mu_V(v)}{\sum_{s_1, s_2} \bar{\mu}(s_1, v, s_2)\, a(s_1) c(s_2)\, e^{\Delta_M(s_1, v)(s_2 - s_1) + \Delta_C(s_1, v)(L(s_2/s_1) - v^2)}},$$

$$c(s_2) \leftarrow \frac{\mu_2(s_2)}{\sum_{s_1, v} \bar{\mu}(s_1, v, s_2)\, a(s_1) q(v)\, e^{\Delta_M(s_1, v)(s_2 - s_1) + \Delta_C(s_1, v)(L(s_2/s_1) - v^2)}}.$$

   Refresh $\mu(s_1, v, s_2)$ using the Gibbs map above.

(b) **Conditional Newton/LM enforcement:** for each $(s_1, v) \in \mathcal{S}_1 \times \mathcal{V}$ do

i. repeat up to inner iterations:

$$w_{s_1,v}(s_2) \;=\; \frac{\mu(s_1, v, s_2)}{\sum_{u \in \mathcal{S}_2} \mu(s_1, v, u)}$$

(conditional law over s_2), residuals

$$r_M(s_1, v) = \sum_{s_2} w_{s_1,v}(s_2)(s_2 - s_1), \qquad r_C(s_1, v) = \sum_{s_2} w_{s_1,v}(s_2)\big(L(s_2/s_1) - v^2\big),$$

Jacobian entries

$$J_{11} = \mathrm{Var}_w(s_2 - s_1), \quad J_{22} = \mathrm{Var}_w\big(L(s_2/s_1) - v^2\big),$$

$$J_{12} = J_{21} = \mathrm{Cov}_w\big(s_2 - s_1,\; L(s_2/s_1) - v^2\big),$$

solve damped Newton system

$$\begin{pmatrix} J_{11} + \lambda & J_{12} \\ J_{21} & J_{22} + \lambda \end{pmatrix} \begin{pmatrix} \delta_M \\ \delta_C \end{pmatrix} = - \begin{pmatrix} r_M \\ r_C \end{pmatrix},$$

update multipliers

$$\Delta_M(s_1, v) \leftarrow \Delta_M(s_1, v) + \delta_M, \qquad \Delta_C(s_1, v) \leftarrow \Delta_C(s_1, v) + \delta_C,$$

refresh $\mu(s_1, v, s_2)$.

ii. until $\sqrt{r_M(s_1, v)^2 + r_C(s_1, v)^2} \le \varepsilon_{\text{fin}}$ or inner cap reached.

5. On convergence set $\mu^\star \leftarrow \mu$.

6. **Fisher information.** With sufficient statistics $T_i(x)$ compute

$$H_{ij} = \sum_x \mu^\star(x)\big(T_i(x) - \mathbb{E}_{\mu^\star}[T_i]\big)\big(T_j(x) - \mathbb{E}_{\mu^\star}[T_j]\big), \quad x = (s_1, v, s_2).$$

7. **Return:** $\mu^\star, H$.

6.2 POT Risk Computation: The Linear Response (LR) Approach

We compute first-order (Gâteaux) price sensitivities under small marginal perturbations using the Fisher information matrix from the calibrated exponential family. Let $\mu^\star$ denote the calibrated coupling, H the Fisher matrix, and h the perturbation vector (12). As shown in Section 5.4, the VIX marginal component h_V is fully determined by the SPX shock via the SSR rule (52). The constraint operator $\mathcal{A}$, the Fisher matrix H, and the dual structure are unchanged; the SSR rule acts only on the construction of h.

The financial constraints are preserved automatically: since the financial block of h is zero by construction (12), the variation $\delta\mu = (\mu^\varepsilon - \mu^\star)/\varepsilon$ satisfies $\mathcal{A}_{\text{fin}}\delta\mu = 0$ as a consequence of the perturbed problem structure (13); no projection of h is needed or meaningful.

Let the payoff be $G : \mathcal{X} \to \mathbb{R}$ with price $\Pi(\varepsilon) = \mathbb{E}_{\mu^\varepsilon}[G]$ and baseline $\Pi(0) = \mathbb{E}_{\mu^\star}[G]$. The first-order risk is

$$\Pi'(0) \;=\; g^\top \dot\theta,$$

where $\dot\theta$ solves the linear response system $H\,\dot\theta = h$, and g is the covariance vector of G with the sufficient statistics.

Inputs. Calibrated coupling $\mu^\star$; Fisher matrix H; full perturbation vector $h = (h_1, h_V, h_2, \mathbf{0}) \in \mathbb{R}^K$ (12); payoff $G(x)$; optional damping $\lambda \geq 0$ and solver tolerances.

Outputs. First-order risk $\Pi'(0)$; optionally the dual variation $\dot{\theta}^0$ (for greeks attribution).

Algorithm 2: Linear Response (LR) Risk Computation.

1. **Solve the regularized linear response system.** Compute the dual variation by solving

$$(H + \lambda I)\,\dot{\theta}^0 \;=\; h,$$

where $\lambda \geq 0$ is a Tikhonov regularization parameter. By Lemmas 2.7–2.8 and Theorem 3.5, the price sensitivity $g^\top \dot{\theta}$ converges to $g^\top H^+ h$ as $\lambda \downarrow 0$, because $g \in \mathrm{range}(H)$ annihilates the λ^{-1} null-space component of $(H+\lambda I)^{-1}h$. In practice, $\lambda > 0$ suppresses amplification of near-null directions of H and controls numerical stability; $\lambda = 0$ recovers the exact pseudoinverse solution when H is numerically well-conditioned. Use the same gauge as in calibration.

2. **Compute the covariance vector g.** Let $\{T_i\}$ be the sufficient statistics (coordinates of the dual potentials). Compute

$$g_i \;=\; \sum_{x \in X} \mu^\star(x) \Big(G(x) - \mathbb{E}_{\mu^\star}[G]\Big) \Big(T_i(x) - \mathbb{E}_{\mu^\star}[T_i]\Big), \qquad i = 1, \ldots, \dim(\theta).$$

3. **Evaluate first-order risk.**

$$\Pi'(0) \;=\; g^\top \dot{\theta}^0.$$

Return $\Pi'(0)$ (and $\dot{\theta}^0$ if needed for greeks attribution).

Notes.

- The covariance step can be reused across multiple payoffs once $\mu^\star$ and $\{T_i\}$ are fixed; only g changes with G.

7 Dimensional Reduction (DR) For POT

An alternative to computing first-order sensitivities via the Fisher information is to exploit the conditional coupling invariance directly and re-solve a reduced entropic projection on (S_1, V). Under a conditional kernel invariance assumption, the perturbed three-dimensional problem is equivalent to a two-dimensional entropic projection for γ on (S_1, V), so one may obtain the exact perturbed coupling in the reduced class by solving a Sinkhorn-type projection that matches the perturbed VIX marginal implied by the SSR propagation of the SPX shock, while remaining close in entropy to the base reduced coupling. This reduced-OT approach retains convexity and numerical stability and, unlike the Fisher linearization, captures nonlinear effects for finite (non-infinitesimal) shocks insofar as the dimension reduction assumption remains numerically accurate.

7.1 Base Conditional Structure

Let $\mu^\star \in \Delta(\mathcal{X})$ denote the calibrated optimal coupling on $\mathcal{X} = \mathcal{S}_1 \times \mathcal{V} \times \mathcal{S}_2$. Define its (S_1, V)-marginal and the conditional kernel of S_2 given (S_1, V) by

$$\gamma^\star(s_1, v) := \sum_{s_2 \in \mathcal{S}_2} \mu^\star(s_1, v, s_2), \qquad \kappa^\star(s_2 \mid s_1, v) := \frac{\mu^\star(s_1, v, s_2)}{\gamma^\star(s_1, v)},$$

so that the coupling admits the disintegration

$$\mu^\star(s_1, v, s_2) = \kappa^\star(s_2 \mid s_1, v)\, \gamma^\star(s_1, v).$$

7.2 Conditional Coupling Invariance Assumption

Assumption 7.1 (Conditional Coupling Invariance). Under sufficiently small perturbations of the SPX marginals, the conditional distribution of S_2 given (S_1, V) remains unchanged, i.e.,

$$\kappa^{\varepsilon}(s_2 \mid s_1, v) = \kappa^{\star}(s_2 \mid s_1, v) \quad \text{for all } (s_1, v, s_2).$$

This assumption reflects that the structural dependence between S_2 and (S_1, V) is stable under small marginal shocks.

Remark (S_2 marginal under DR: endogeneity and LR comparison). Under Assumption 7.1, the S_2 marginal of the perturbed coupling is fully determined by $\kappa^{\star}$ and γ^{ε}:

$$\mu_2^{DR}(s_2) \;=\; \sum_{s_1, v} \kappa^{\star}(s_2 \mid s_1, v)\, \gamma^{\varepsilon}(s_1, v).$$

This is an *endogenous* output of the DR method, not an independently prescribed target. If a spot or volatility bump prescribes an exogenous $\mu_2^{\varepsilon} \neq \mu_2^{DR}$, then the assumption and the exogenous target are generically incompatible: enforcing both would require perturbing $\kappa^{\star}$. The DR method therefore matches μ_1^{ε} and μ_V^{ε} exactly, and accepts μ_2^{DR} as the best $\kappa^{\star}$-consistent approximation to μ_2^{ε}.

By contrast, the *Linear Response* (LR) method enforces all three marginal targets $(\mu_1^{\varepsilon}, \mu_V^{\varepsilon}, \mu_2^{\varepsilon})$ as independent inputs to the Fisher system $H\dot{\theta}^0 = h$. The gap between the two treatments is $O(\varepsilon)$:

$$\mu_2^{\varepsilon}(s_2) - \mu_2^{DR}(s_2) \;=\; \varepsilon\big[h_2(s_2) - (L_{\kappa^{\star}}\dot{\gamma}^0)(s_2)\big] + O(\varepsilon^2),$$

where $L_{\kappa^{\star}}\dot{\gamma}^0(s_2) := \sum_{s_1, v} \kappa^{\star}(s_2 \mid s_1, v)\dot{\gamma}^0(s_1, v)$. The compatibility condition $h_2 = L_{\kappa^{\star}}\dot{\gamma}^0$ that would make the leading term vanish does not hold for generic market bumps. The close LR–DR agreement across VIX futures and options in Section 8.3 confirms that this gap is small in practice.

7.3 Exact Dimensional Reduction

Theorem 7.2 (Exact Reduction to Two-Dimensional Entropic Projection). Assume $\mu^{\star}$ is strictly positive on $\mathcal{X}$ and Assumption 7.1 holds.

Then the perturbed entropic projection problem

$$\inf_{\mu \in \mathcal{P}^{\varepsilon}} D(\mu \,\|\, \mu^{\star})$$

reduces exactly to the two-dimensional problem

$$\inf_{\gamma \in \mathcal{Q}^{\varepsilon}} D(\gamma \,\|\, \gamma^{\star}),$$

where $\mathcal{Q}^{\varepsilon}$ is the set of probability measures γ on $\mathcal{S}_1 \times \mathcal{V}$ satisfying the perturbed (S_1, V)-marginal constraints:

$$\mathcal{Q}^{\varepsilon} \;:=\; \Big\{\gamma \in \Delta(\mathcal{S}_1 \times \mathcal{V}) :\; \textstyle\sum_v \gamma(s_1, v) = \mu_1^{\varepsilon}(s_1),\; \sum_{s_1} \gamma(s_1, v) = \mu_V^{\varepsilon}(v)\Big\}. \tag{54}$$

The S_2 marginal is *endogenous*: it is determined as $\mu_2^{DR}(s_2) = \sum_{s_1, v} \kappa^{\star}(s_2 \mid s_1, v)\gamma^{\varepsilon}(s_1, v)$ rather than independently prescribed (see Remark 7.2). The full three-dimensional coupling is reconstructed by

$$\mu^{\varepsilon}(s_1, v, s_2) = \kappa^{\star}(s_2 \mid s_1, v)\, \gamma^{\varepsilon}(s_1, v).$$

Proof. Consider the restricted class of couplings that share the base conditional kernel $\kappa^{\star}$:

$$\mathcal{R}^{\varepsilon} \;:=\; \big\{\, \mu \in \mathcal{P}^{\varepsilon} : \mu(s_1, v, s_2) = \kappa^{\star}(s_2 \mid s_1, v)\, \gamma(s_1, v) \text{ for some probability measure } \gamma \text{ on } \mathcal{S}_1 \times \mathcal{V} \,\big\}.$$

By Assumption 7.1, the optimizer of the full problem $\inf_{\mathcal{P}^\varepsilon} D(\mu\|\mu^\star)$ has its conditional kernel equal to $\kappa^\star$ for all sufficiently small ε; hence it belongs to $\mathcal{R}^\varepsilon$. The full infimum therefore coincides with the restricted infimum:

$$\inf_{\mu\in\mathcal{P}^\varepsilon} D(\mu\|\mu^\star) \;=\; \inf_{\mu\in\mathcal{R}^\varepsilon} D(\mu\|\mu^\star).$$

It now suffices to evaluate the entropy for any $\mu \in \mathcal{R}^\varepsilon$. Writing $\mu(s_1, v, s_2) = \kappa^\star(s_2 \mid s_1, v)\,\gamma(s_1, v)$ and substituting into the relative entropy:

$$D(\mu^\varepsilon \,\|\, \mu^\star) = \sum_{s_1,v,s_2} \mu^\varepsilon(s_1, v, s_2) \ln \frac{\mu^\varepsilon(s_1, v, s_2)}{\mu^\star(s_1, v, s_2)}.$$

Using the disintegration formulas for μ^ε and $\mu^\star$:

$$= \sum_{s_1,v,s_2} \kappa^\star(s_2 \mid s_1, v)\,\gamma(s_1, v) \ln \frac{\kappa^\star(s_2 \mid s_1, v)\,\gamma(s_1, v)}{\kappa^\star(s_2 \mid s_1, v)\,\gamma^\star(s_1, v)}.$$

Canceling $\kappa^\star(s_2 \mid s_1, v)$ inside the logarithm yields

$$= \sum_{s_1,v,s_2} \kappa^\star(s_2 \mid s_1, v)\,\gamma(s_1, v) \ln \frac{\gamma(s_1, v)}{\gamma^\star(s_1, v)}.$$

Since for each (s_1, v), $\sum_{s_2} \kappa^\star(s_2 \mid s_1, v) = 1$, we obtain

$$D(\mu^\varepsilon \,\|\, \mu^\star) = \sum_{s_1,v} \gamma(s_1, v) \ln \frac{\gamma(s_1, v)}{\gamma^\star(s_1, v)} = D(\gamma \,\|\, \gamma^\star).$$

Thus the three-dimensional projection problem is equivalent to the two-dimensional entropic projection.

The perturbed constraints on μ reduce to the (S_1, V)-marginal constraints (54) on γ; the S_2 marginal is determined endogenously by $\kappa^\star\gamma^\varepsilon$. The reconstructed coupling preserves the conditional martingale and variance-consistency relations inherited from the base calibration, since these depend only on the fixed conditional kernel $\kappa^\star$. □

Computational implication. In the base calibration, the entropic martingale optimal transport problem must enforce the martingale constraint $\mathbb{E}[S_2|S_1, V] = S_1$, which couples all three variables and requires a full three-dimensional Sinkhorn calibration. By Theorem 7.2, the perturbed problem requires no such re-imposition: operationally it amounts to running a two-marginal Sinkhorn projection on (S_1, V) *without re-imposing the martingale constraint*, with $\kappa^\star$ carrying the financial constraints forward automatically.

This is the key reason why risk generation under DR is computationally efficient: the perturbed problem no longer requires recalibration of the full martingale optimal transport model. In practice the perturbed projection typically converges in only 5–6 Sinkhorn iterations because the solution is close to the base coupling.

7.4 SPX–VIX Family Risk Generation: The Dimensional Reduction (DR) Approach

We now describe the practical algorithm used to compute SPX–VIX risk sensitivities under SSR while preserving the structure of the calibrated joint coupling $\mu^\star(s_1, v, s_2)$ from Section 6.1, which by construction satisfies the SPX and VIX market constraints, the martingale condition, and the SPX–VIX consistency condition. The key point is that the perturbation is not generated by directly changing the SPX marginal inside the transport problem. Rather, one starts from an exogenous SPX market shock (a spot or volatility bump), propagates it through the SSR dynamics to obtain the corresponding change in VIX option prices, and uses these to define a new VIX marginal target. Rather than fully recalibrating the joint coupling, which would be computationally expensive, we exploit the dimension reduction result of Section 7: the perturbation

is carried out at the level of the lower-dimensional coupling on (S_1, V) while leaving the conditional kernel of S_2 given (S_1, V) unchanged.

More precisely, write the base calibrated coupling in disintegrated form as

$$\mu^\star(s_1, v, s_2) = \gamma^\star(s_1, v)\, \kappa^\star(s_2 \mid s_1, v),$$

where $\gamma^\star(s_1, v)$ is the marginal coupling of (S_1, V) and $\kappa^\star(s_2 \mid s_1, v)$ is the conditional kernel of S_2 given (S_1, V). By the dimension reduction theorem, the perturbed coupling is constructed by updating only $\gamma^\star$ while holding $\kappa^\star$ fixed:

$$\mu_\varepsilon(s_1, v, s_2) = \gamma^\varepsilon(s_1, v)\, \kappa^\star(s_2 \mid s_1, v).$$

The VIX marginal therefore adjusts through the perturbation of γ^ε, while the conditional dependence structure of S_2 given (S_1, V) remains inherited from the base calibration.

Algorithm 3: SSR-Enhanced Dimensional Reduction (DR) For POT Risk Generation

1. **Inputs.**
   - Base joint coupling $\mu^\star(s_1, v, s_2)$ and relevant marginals from Algorithm 1
   - Exogenous SPX perturbation (e.g., spot bump or volatility surface shift)
   - SSR (Skew Stickiness Ratio) parameters for VIX volatility dynamics
   - Observed SPX and VIX market data
2. **Outputs.**
   - Updated perturbed coupling $\mu^\varepsilon(s_1, v, s_2)$
   - Risk sensitivities under μ_ε
3. **Base Calibration.**
   (a) Disintegrate $\mu^\star$ as
   $$\mu^\star(s_1, v, s_2) = \gamma^\star(s_1, v)\, \kappa^\star(s_2 \mid s_1, v),$$
   where $\gamma^\star$ is the (S_1, V) marginal and $\kappa^\star$ is the conditional kernel.
4. **Generate exogenous SPX perturbation.**
   (a) Apply the prescribed SPX perturbation (e.g., spot or implied volatility shift) to obtain the new SPX marginal and updated SPX implied forward variance F'_V.
5. **Propagate VIX smile using SSR.**
   (a) Apply the SSR rule (43) to obtain the perturbed VIX implied volatility surface $\sigma'_{\mathrm{VIX}}(K)$.
   (b) Compute the corresponding perturbed VIX option prices from the shifted surface.
6. **Construct perturbed VIX marginal.**
   (a) Infer the new VIX marginal distribution so that, under the VIX variable, the model reproduces the SSR-propagated VIX option prices.
7. **Dimension-reduced entropic transport update.**
   (a) Holding $\kappa^\star(s_2 \mid s_1, v)$ fixed, solve the two-dimensional entropic projection (54): find $\gamma^\varepsilon \in \mathcal{Q}^\varepsilon$ closest in $D(\cdot\|\gamma^\star)$, where $\mathcal{Q}^\varepsilon$ enforces the perturbed *SPX* T_1 *marginal* μ_1^ε (from the SPX shock) and the perturbed *VIX marginal* μ_V^ε (from the SSR propagation). The S_2 marginal is *not* independently constrained; it is determined endogenously as $\mu_2^{DR}(s_2) = \sum_{s_1, v} \kappa^\star(s_2 \mid s_1, v)\gamma^\varepsilon(s_1, v)$ (see Remark 7.2).

(b) Reconstruct the full perturbed joint coupling as

$$\mu_\varepsilon(s_1, v, s_2) = \gamma^\varepsilon(s_1, v)\, \kappa^\star(s_2 \mid s_1, v).$$

8. **Risk extraction.**

(a) For any payoff function G, compute model prices under $\mu^\star$ and μ_ε, and report the sensitivity as

$$\text{Greek} \approx \frac{P(\mu_\varepsilon) - P(\mu^\star)}{\varepsilon},$$

where $P(\mu)$ denotes the portfolio valuation under μ.

This procedure avoids a full recalibration of the original SPX–VIX martingale optimal transport problem. The perturbation is carried only by the reduced coupling in (S_1, V), while the conditional kernel of S_2 given (S_1, V) remains unchanged. In this way, the endogenous adjustment of the VIX marginal is captured through the perturbed reduced coupling, yielding a fast and structurally consistent risk-generation algorithm.

8 Experiments: SPX-VIX Risk Generation And Hedging Backtest

8.1 SPX–VIX Basis In Market Data

In theory the VIX future level should be consistent with the forward variance implied by the SPX option surface through the well-known replication formula. This is precisely the consistency condition in (2). However, empirical market data shows that this relation does not hold exactly. In practice a persistent basis exists between the SPX implied forward variance and the traded VIX futures.

Figure 2 shows the time series of the SPX–VIX basis for the 1-month tenor over a two-year window; this basis is well documented in practice and is typically attributed to market segmentation, liquidity effects, and supply–demand imbalances in the VIX futures market. Our calibration framework therefore allows a basis adjustment when linking SPX forward variance to the VIX future level.

Formal treatment of the basis. Define the pointwise SPX–VIX basis at each node (s_1, v) by

$$\eta(s_1, v) \;:=\; v^2 \;-\; \mathbb{E}_{\mu^\star}\big[L(S_2/S_1) \mid S_1 = s_1,\, V = v\big], \tag{55}$$

so that η measures the pointwise gap between the VIX-squared target and the SPX-implied forward variance realized under the calibrated coupling. The consistency relation (2) corresponds to $\eta \equiv 0$; empirically, as documented in Figure 2, η is persistently nonzero due to convexity adjustments, discrete monitoring, and VIX settlement conventions. We therefore replace (2) by the relaxed node-wise target

$$(\mathcal{A}_{\text{fin}}\mu)^C_{ij} \;=\; \sum_{s_2} \mu(s_1^i, v^j, s_2)\,\big(L(s_2/s_1^i) - (v^j)^2 + \eta(s_1^i, v^j)\big) \;=\; 0, \tag{56}$$

i.e. $\mathbb{E}[L(S_2/S_1) \mid S_1, V] = V^2 - \eta(S_1, V)$ at each grid node, with η entering the Gibbs exponent additively through $\Delta_C(s_1, v)$ (Algorithm 1). The basis η is calibrated once from market data (specifically, from the gap between the SPX-implied variance strip and the quoted VIX future at each conditioning node (s_1^i, v^j)), and is treated as a fixed structural offset that does not vary with the market perturbation. It is enforced softly via the financial tolerance ε_{fin} in Algorithm 1: residuals of size $O(\varepsilon_{\text{fin}})$ around the η-shifted target are absorbed by the inner Newton stopping criterion.

Under the spot and volatility perturbations of Section 4, η is held fixed: bumps act only on the marginal targets $(\mu_1^\varepsilon, \mu_V^\varepsilon, \mu_2^\varepsilon)$, so $db_{\text{fin}}^\varepsilon/d\varepsilon = 0$ and the financial slots of the perturbation vector h (12) remain zero. This is appropriate as long as the basis is driven by structural microstructure effects (liquidity, settlement methodology) that do not co-move with small SPX surface perturbations.

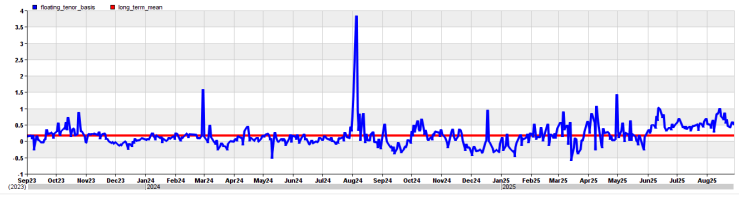

Figure 2: SPX–VIX basis time series for the 1-month tenor over a two-year window.

8.2 Base Calibration And Fit Quality

Despite the SPX–VIX basis noted above, the calibrated optimal transport model satisfies the martingality condition and approximate consistency constraints, as we verify below. We first assess the quality of the base calibration used throughout the experiments. The joint SPX–VIX coupling $\mu^\star$ is obtained via entropic projection with Sinkhorn scaling on the discrete grids. After calibration, we compute the sufficient statistics and the Fisher information matrix H for subsequent risk analysis. Existence, uniqueness, and the Gibbs form of the optimizer ensure a consistent fit to the prescribed marginals and targets on the grids.

To visualize fit quality, we plot observed market smiles against model-implied values from the calibrated coupling for a representative maturity (e.g., March 18, 2026, two weeks to expiry), consistent with our option risk comparisons. Additionally, we generate the martingality plot and consistency plot.

(a) SPX T_1 smile fit

(b) SPX T_2 smile fit

Figure 3: SPX smile fit quality (two expiries)

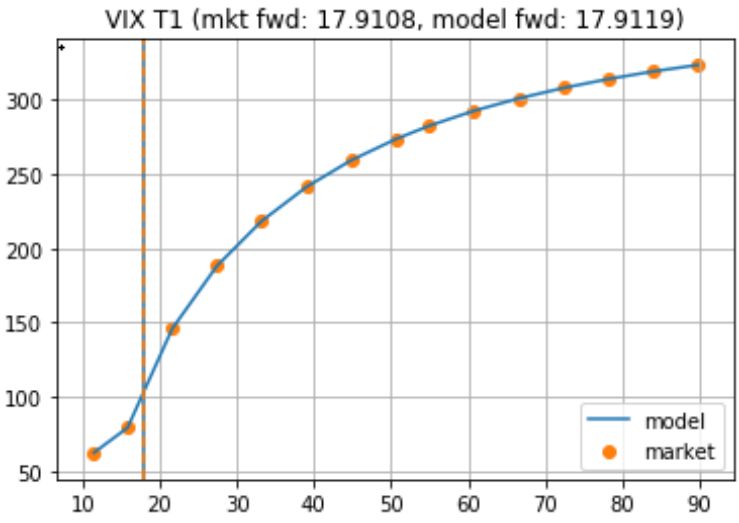

Figure 4: VIX smile fit: observed vs model-implied

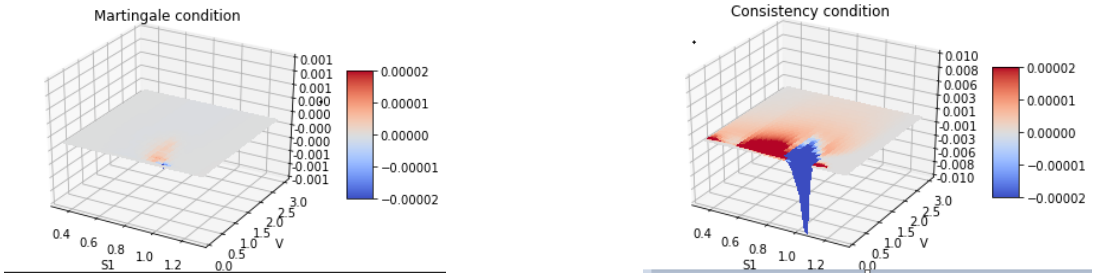

(a) Martingality check

(b) Consistency condition

Figure 5: SPX–VIX calibration theoretical conditions

8.3 Risk Computation Benchmark: Recalibration vs Perturbation

This section evaluates the accuracy and computational efficiency of the perturbation framework developed in the preceding sections by comparing two approaches for computing risk sensitivities under SPX market perturbations.

1. **Full recalibration (benchmark).** After applying a perturbation to the SPX market, the entire SPX–VIX martingale optimal transport calibration problem is recomputed using Algorithm 1. The resulting joint distribution $\mu^{\varepsilon}_{\text{recal}}$ serves as the benchmark distribution for computing option prices and sensitivities.

2. **Perturbation (LR).** Starting from the calibrated base coupling $\mu^{\star}$, we compute the perturbed distribution using the linear response system derived in Sections 3.4–3.5. This method uses the Fisher information matrix of the calibrated exponential family to approximate the perturbed coupling $\mu^{\varepsilon}_{\text{pert}}$ without solving the full calibration problem again.

The goal is twofold: to verify that the perturbation-based sensitivities closely match those from full recalibration, and to demonstrate the significant computational speedup the LR method achieves over repeated full calibration (Table 4).

SPX perturbations. In all experiments the perturbation is applied on the SPX side, either as a spot shift or as a parallel shift of the SPX implied volatility surface. These perturbations are mapped to corresponding changes in the forward variance, which acts as the key control variable in the SPX–VIX coupling.

The perturbations are chosen to remain within a regime where the linear-response approximation is expected to be accurate while still representing realistic market shocks.

Implementation details. Several groups of parameters control the perturbation experiments:

- **Base OT object.** The initial martingale optimal transport calibration provides the reference coupling $\mu^\star$ and the Fisher information matrix used in the perturbation calculations.
- **Bumped SPX information.** The perturbed SPX marginal distributions include the shifted spot and the modified implied volatility surface at the relevant maturities. Throughout the experiments we assume a sticky-strike behavior for the SPX volatility surface under spot perturbations.
- **Perturbation controls.** Parameters defining the magnitude and structure of the volatility perturbations, including lower and upper cutoffs for invariant volatility regions.
- **VIX volatility shape controls.** Parameters governing the Skew Stickiness Ratio (SSR), skewness, convexity, and the treatment of at-the-money and out-of-the-money VIX option strikes.
- **Basis and numerical controls.** Optional parameters allowing forward basis adjustments, regularization parameters, and marking conventions for volatility, skew, SSR, convexity, and VIX marginal constraints.

8.4 VIX Option Risk And Cross-Greeks

Using the experimental setup of Section 8.3, we compare SPX risk sensitivities of VIX derivatives under full recalibration and the LR perturbation method.

VIX future cross-greeks. We begin by comparing the SPX cross-greeks of the VIX future contract. The sensitivities are computed with respect to SPX spot and SPX implied volatility perturbations. Table 1 reports the SPX delta and SPX vega of the VIX future obtained from the recalibration benchmark and from the perturbation method.

Table 1: VIX Future's SPX Greeks: LR-POT vs Recalibration

	LR-POT. SPX Delta	**Recalib. SPX Delta**	**LR-POT. SPX Vega**	**Recalib. SPX Vega**
VIX Future	-8.88339	-8.99380	1043.42832	1071.35419

The results show that the perturbation-based sensitivities closely match those obtained from the full recalibration procedure. The differences remain small relative to the magnitude of the sensitivities, confirming that the linear response (LR) system provides an accurate local approximation of the recalibrated optimal transport model.

VIX option SPX delta. We next compare SPX delta sensitivities for a strip of VIX call options spanning a wide range of strikes. The options correspond to the same expiry used in the calibration experiment and cover both out-of-the-money and near-the-money regions of the VIX smile.

Table 2: VIX Options SPX Delta Comparison (LR-POT vs Recalibration). March 18, 2026, 2w to expiry.

Strike	Pert. Delta	Recalib. Delta
16.9	−0.786	−0.809
17.6	−0.750	−0.763
18.2	−0.714	−0.719
18.7	−0.680	−0.674
19.2	−0.641	−0.629
19.7	−0.601	−0.585
20.3	−0.559	−0.540
20.9	−0.516	−0.495
21.6	−0.469	−0.450
22.5	−0.420	−0.405
23.5	−0.369	−0.360
24.7	−0.316	−0.315
26.3	−0.266	−0.270
28.5	−0.221	−0.225
31.4	−0.178	−0.179
35.8	−0.133	−0.135
44.0	−0.089	−0.090

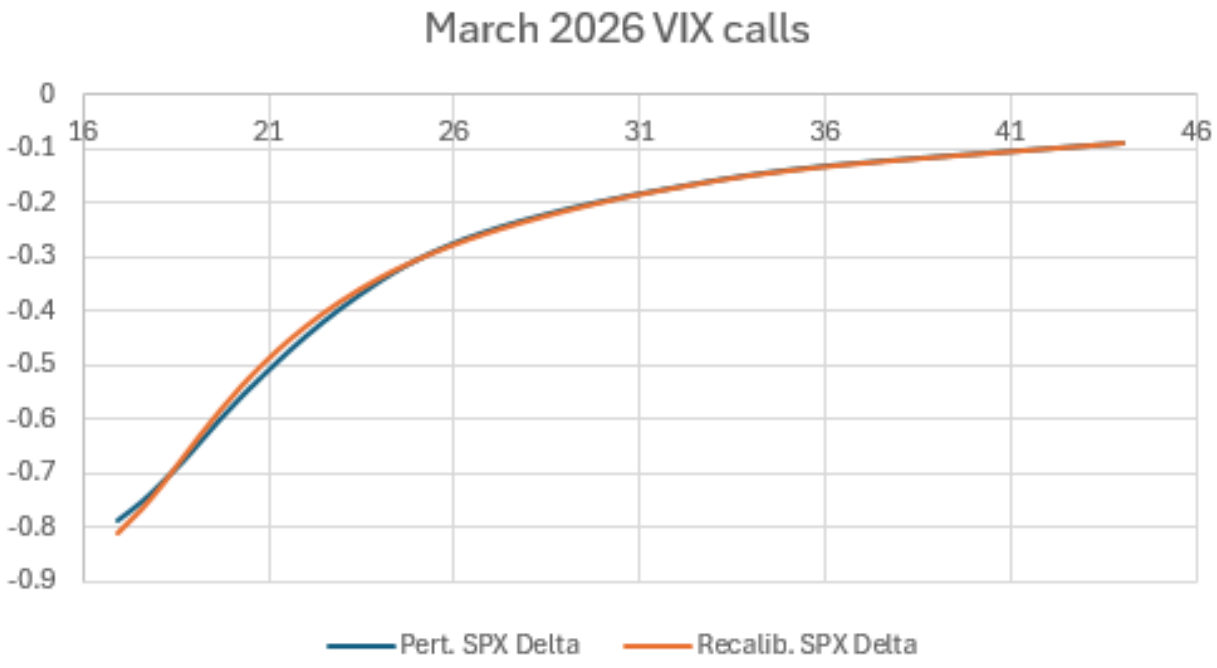

Figure 6: SPX Delta

Figure 6 visualizes the same comparison across strikes.

The perturbation-based deltas closely track the sensitivities obtained from the full recalibration. Small discrepancies appear primarily in the wings of the VIX smile, where nonlinear effects become more pronounced. However, even in these regions the overall shape and magnitude of the sensitivities remain consistent with the recalibration benchmark.

VIX option SPX vega. We perform the same comparison for SPX vega sensitivities of the VIX options. Table 3 reports the SPX vega obtained from both approaches.

Table 3: VIX Options SPX Vega Comparison (LR-POT vs Recalibration). March 18, 2026, 2w to expiry.

Strike	Pert. Vega	Recalib. Vega
16.9	94.452	96.675
17.6	90.136	91.291
18.2	85.485	86.048
18.7	81.221	80.708
19.2	76.337	75.456
19.7	71.155	70.103
20.3	65.942	64.734
20.9	60.749	59.364
21.6	55.294	53.985
22.5	50.338	48.601
23.5	45.134	43.213
24.7	39.681	37.821
26.3	34.065	32.419
28.5	28.130	27.014
31.4	21.819	21.568
35.8	15.672	16.206
44.0	10.432	10.800

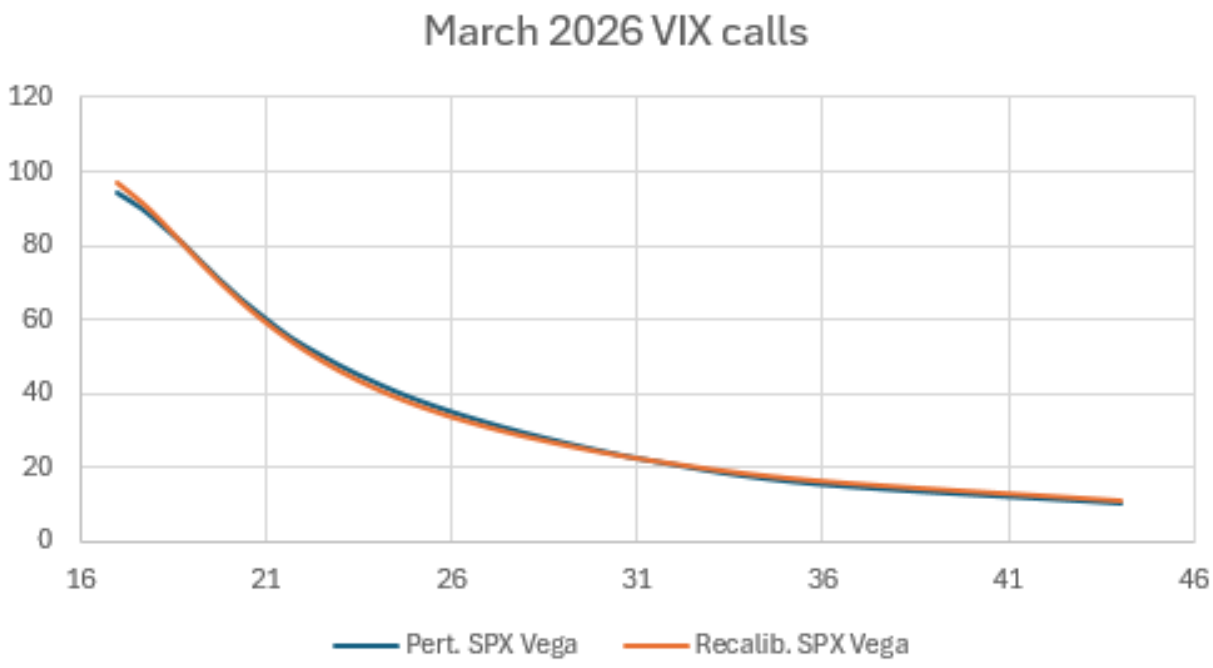

Figure 7: SPX Vega

As with the delta comparison, the perturbation method reproduces the recalibrated sensitivities with high accuracy. The agreement confirms that the Fisher-information linear response captures the dominant first-order effects of SPX volatility perturbations on VIX option prices.

Performance comparison. While the recalibration method provides the benchmark sensitivities, it requires solving the full SPX–VIX optimal transport calibration problem after each perturbation. This involves repeated Sinkhorn iterations together with enforcement of the martingale and variance-consistency constraints, making the computation relatively expensive.

Table 4: Risk Performance Comparison

Base calibration	Recalib based risk calculation	DR-POT method	LR-POT method
348.26 s	370.13 s	18.45 s	5.73 s

Table 4 compares the runtime required to compute sensitivities under the three approaches. The results show that the LR method and the DR method both achieve orders-of-magnitude speedups ($\sim$60$\times$ and $\sim$20$\times$ respectively; see Table 4) while maintaining accuracy comparable to the recalibration benchmark.

This efficiency gain is the key practical advantage of the perturbation framework: risk sensitivities can be generated quickly without re-running the full martingale optimal transport calibration.

Lastly, we note that the risk numbers generated by the DR method (Section 7) are extremely close to those produced by the LR method. This agreement is non-trivial: as discussed in Remark 7.2, the two methods treat the S_2 marginal differently: LR enforces the prescribed μ_2^ε directly, while DR treats it as endogenous under the fixed conditional kernel $\kappa^\star$. The close agreement provides empirical validation that Assumption 7.1 is a good approximation in the market environments tested, i.e. that $\mu_2^{DR} \approx \mu_2^\varepsilon$ to within risk-relevant accuracy.

8.5 Backtest: Hedging Efficiency Of Optimal Transport Method

We now evaluate whether the SPX sensitivities produced by our model independent risk generation methods lead to more effective hedging than those generated by a benchmark industry standard model, in this case a stochastic local volatility model. In the backtest we perform below, we choose the dimensional reduction (DR) method, Algorithm 3.

The experiment consists of two parts: a first hedging backtest in which portfolios of VIX options are hedged using VIX futures; and a second hedging backtest in which the same option portfolio is hedged using SPX futures and SPX vanillas. The sizing of the VIX futures is determined by matching SPX Vega computed under either the optimal transport method or the stochastic local volatility (SLV) benchmark. The sizing of the SPX futures and SPX vanillas is similarly determined by matching SPX delta and SPX vega between the hedging instruments and the VIX option portfolio for each of the methods. Because the two methodologies trade comparable notionals, we omit transaction costs.

Backtest period The backtest runs daily from January 2024 to February 2026. VIX smile dynamics follow the SSR rule (43) with $\beta_V = 1.2$.

Synthetic portfolio generation To test the robustness of the hedging performance we generate 50 randomized VIX option portfolios.

For each trading day t the portfolios are constructed as follows:

1. All listed VIX expiries available on day t are included.
2. For each expiry we construct a strike grid using call option deltas

$$\Delta \in \{10, 15, \ldots, 90\},$$

   resulting in 17 strikes per maturity.
3. Options with $\Delta < 50$ are taken as puts while options with $\Delta \geq 50$ are taken as calls.

4. Each option i is assigned a random portfolio weight

$$w_{i,t} \sim \text{Uniform}(-1, 1).$$

The resulting portfolio value is

$$P_t = \sum_i w_{i,t} V_{i,t}.$$

This procedure produces diversified portfolios spanning a wide range of smile exposures.

Hedging methodology The portfolios are hedged using VIX futures whose expiries match those of the VIX options. The hedge sizes are determined by matching SPX Vega per expiry.

For a given model $M \in \{\text{SLV}, \text{POT}\}$ we compute

$$G_t^M = \frac{\partial P_t}{\partial \sigma_{SPX}},$$

the SPX sensitivity of the option portfolio, and

$$g_{j,t}^M = \frac{\partial F_{j,t}}{\partial \sigma_{SPX}},$$

the SPX sensitivity of each VIX future $F_{j,t}$.

The hedge sizes $\alpha_{j,t}^M$ are chosen so that

$$G_t^M + \sum_j \alpha_{j,t}^M g_{j,t}^M = 0.$$

Hedged P&L The daily hedged P&L for model M is

$$P\&L_t^M = \Delta P_t + \sum_j \alpha_{j,t}^M \Delta F_{j,t}.$$

The effectiveness of the hedge is evaluated using the standard deviation of the hedged P&L.

Cross-sectional comparison across portfolios For each of the 50 randomly generated portfolios we compute the standard deviation of the hedged P&L under both hedging strategies.

Figure 8 plots the difference

$$\sigma_{POT} - \sigma_{SLV}$$

for each portfolio, where σ_{POT} and σ_{SLV} denote the standard deviation of hedged P&L under the POT and SLV hedges, respectively.

Time-series hedge stability To illustrate the time-series behavior of the hedging error, we select one representative portfolio from the set of 50 portfolios and compute the rolling 20-day standard deviation of hedged P&L.

$$\text{RollStdev}_t^M(20) = \sqrt{\frac{1}{19} \sum_{u=t-19}^{t} \left(P\&L_u^M - \overline{P\&L}_{t,20}^M \right)^2}.$$

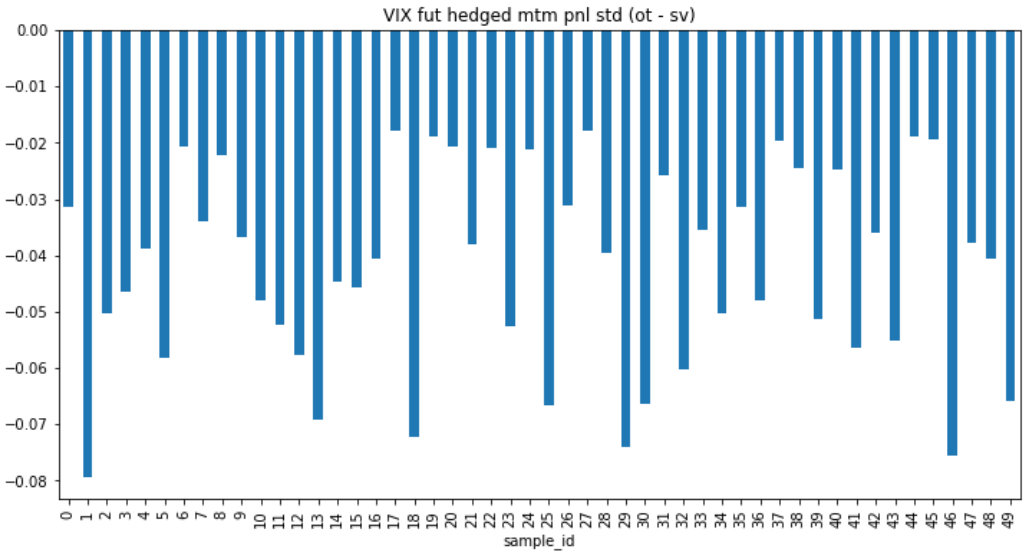

Figure 8: Difference in hedged P&L standard deviation between the POT hedge and the SLV hedge across 50 randomized VIX option portfolios using VIX futures. Each bar corresponds to one portfolio. Negative values indicate that the POT hedge achieves lower hedging variance than the SLV hedge.

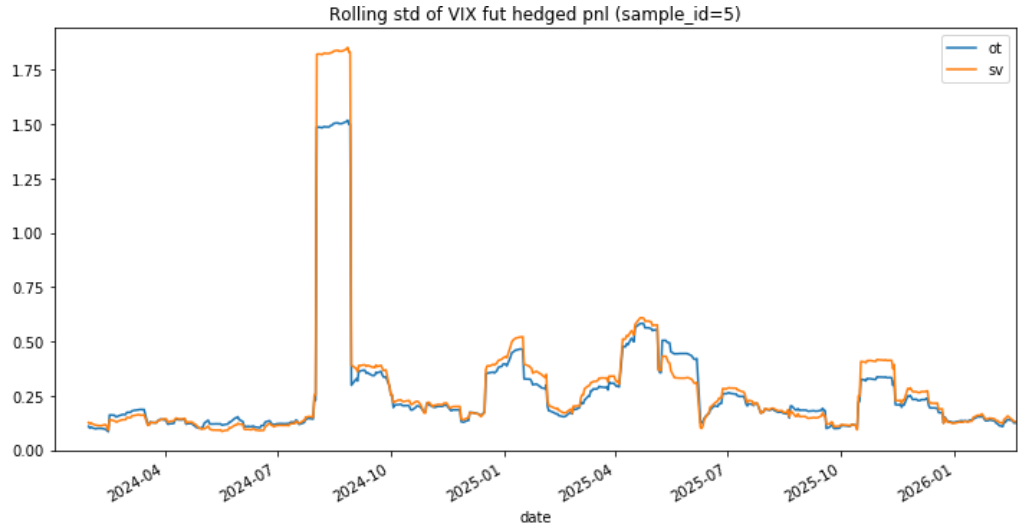

Figure 9: 20-day rolling standard deviation of VIX future hedged P&L for a representative portfolio. The POT hedge produces lower hedging variance during volatile periods while remaining comparable to the SLV hedge during calm market regimes.

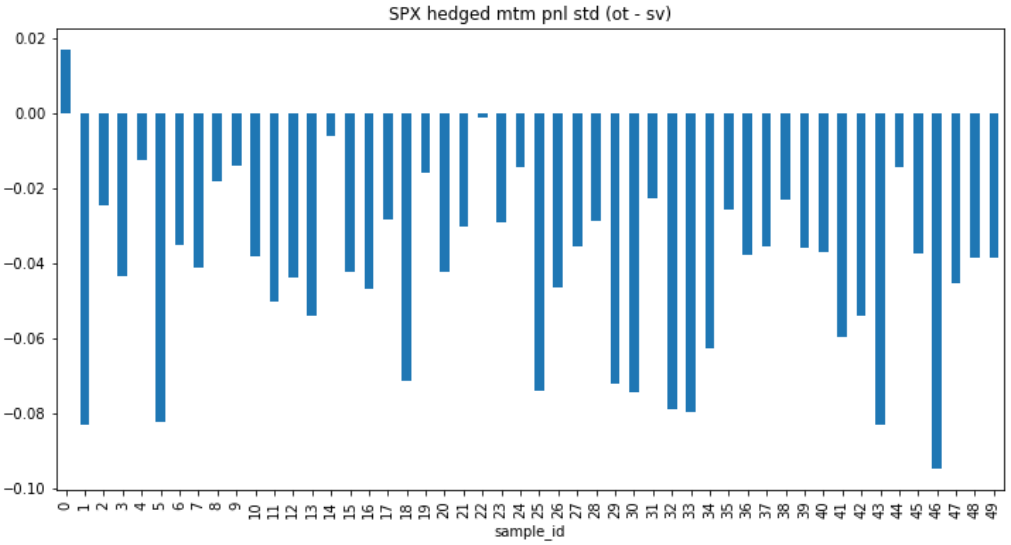

Figure 10: Difference in hedged P&L standard deviation between the POT hedge and the SLV hedge across 50 randomized VIX option portfolios using SPX futures and SPX vanillas. Each bar corresponds to one portfolio. Negative values indicate that the POT hedge achieves lower hedging variance than the SLV hedge.

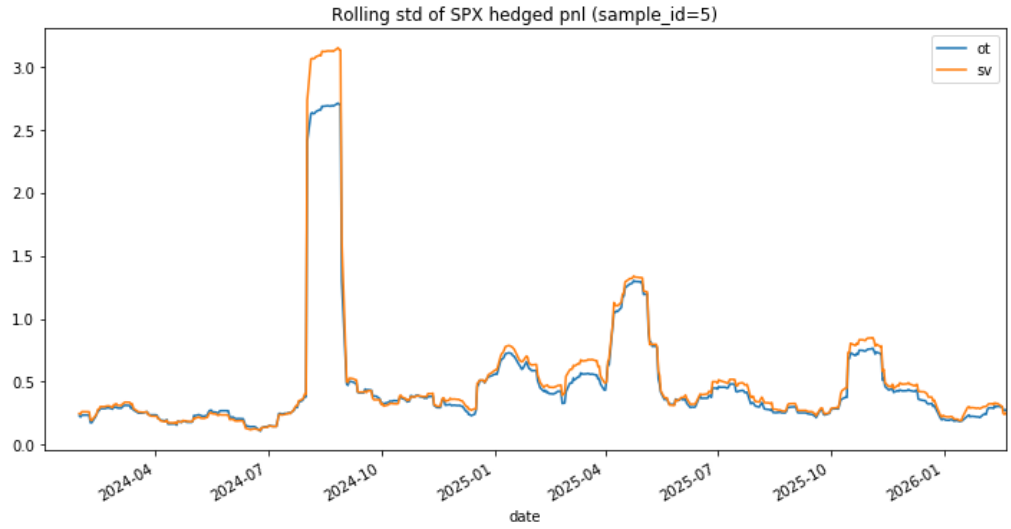

Figure 11: 20-day rolling standard deviation of SPX future and SPX vanillas hedged P&L for a representative portfolio. The POT hedge produces lower hedging variance during volatile periods while remaining comparable to the SLV hedge during calm market regimes.

Summary The cross-sectional experiment in Figure 8 shows that the POT VIX future hedge reduces PnL variance for all tested portfolios. In Figure 10, all but one of the 50 VIX option portfolios have smaller PnL variance for the POT method when hedged to SPX futures and SPX vanillas. The time-series analysis in both Figure 9 and Figure 11 further demonstrates that the improvement is most pronounced during periods of elevated market volatility.

Together these results provide empirical evidence that the perturbed optimal transport framework produces more accurate SPX–VIX risk sensitivities than a benchmark stochastic local volatility model.

9 Payoff-Agnostic Risk: A VIX-Barrier Forward-Starting Option

The risk representation of Theorem 3.5 holds for any payoff $G : \mathcal{X} \to \mathbb{R}$, not only VIX vanillas. To illustrate this generality we price and risk a forward-starting SPX call whose knock-in is contingent on the VIX level at T_1: the return leg $\max(S_2/S_1 - 1, 0)$ carries no explicit VIX dependence, yet the VIX-conditional barrier couples the payoff directly to the VIX marginal. This exotic exercises the full three-way structure of (S_1, V, S_2) and shows that a single Fisher linear solve suffices to risk it.

Setup. We value on 2026-03-02 with $T_1 =$ 2026-03-18 and $T_2 =$ 2026-04-17. The SPX spot is $S_0 = 6881.62$, with forwards $F_1 = 6888.80$ at T_1 and $F_2 = 6908.70$ at T_2; the VIX future at T_1 is $F_V = 20.93$. We compare two payoffs on $\mathcal{X} = \mathcal{S}_1 \times \mathcal{V} \times \mathcal{S}_2$,

$$G_{\text{van}}(S_1, V, S_2) = \max\big(S_2/S_1 - 1,\, 0\big), \tag{57}$$

$$G_{\text{bar}}(S_1, V, S_2) = \max\big(S_2/S_1 - 1,\, 0\big) \cdot \mathbf{1}_{\{V>25\}}, \tag{58}$$

an at-the-money forward-starting SPX call (57) and the same call knocked in only when VIX exceeds 25 at T_1 (58).

Pricing. Table 5 reports the two prices under the calibrated coupling $\mu^\star$. The barrier removes 89.20% of probability mass (the scenarios with $V \le 25$), reducing the price by 73.4%. At current levels ($F_V = 20.93 < 25$) the knock-in sits above the VIX future in the upper tail, so the activation probability is only 10.80%.

Table 5: Pricing of the forward-starting SPX call and its VIX-barrier variant under $\mu^\star$.

Payoff	Price (PV)	Barrier activation
Vanilla forward starting	0.019205	100%
VIX $>$ 25 barrier	0.005117	10.80%

Risk via the Fisher linear solve. Both payoffs are risked from the same dual variation $\dot\theta^0 = H^+ h$, computed once with the variance-anchored h_V and SSR propagation ($\beta_V = 1.2$) of Section 5.4. The payoff-specific sensitivity is $\Pi'(0) = g_G^\top \dot\theta^0$ with $g_G = \mathrm{Cov}_{\mu^\star}(G, T)$. Table 6 reports the SPX delta Δ and SPX vega V_{SPX} of the two payoffs.

The barrier amplifies the delta: because $\mathbf{1}_{\{V>25\}}$ is directly sensitive to the VIX distribution, a spot increase raises F_V through the forward variance and shifts $P(V > 25)$. With the barrier above the VIX future ($F_V = 20.93 < 25$) the knock-in activates only 10.80% of the time, so even modest VIX shifts driven by the spot bump have a large relative impact on barrier activation, giving $|\Delta_{\text{bar}}| > |\Delta_{\text{van}}|$. The vegas differ materially: $\mathcal{V}_{\text{bar}} = 0.001511$ versus $\mathcal{V}_{\text{van}} = 0.001114$ in absolute terms, and 29.52% versus 5.80% of price respectively. A parallel vol shift widens the VIX distribution, pushing substantial mass across the $V = 25$ gate; at 10.80% activation this additional probability is large relative to the option price, producing the high relative vega.

Table 6: SPX Greeks of the forward-starting call and its VIX-barrier variant, from the shared Fisher linear solve.

Metric	Vanilla forward starting	VIX > 25 barrier
Price (PV)	0.019205	0.005117
SPX Δ (per \$1 spot)	-9.25×10^{-6}	-1.32×10^{-5}
SPX Δ (% of price)	-0.05%	-0.26%
SPX $\mathcal{V}$ (per vol pt)	0.001114	0.001511
SPX $\mathcal{V}$ (% of price)	5.80%	29.52%

Scale invariance and variance consistency. The forward return $\max(S_2/S_1 - 1, 0)$ is algebraically scale-invariant: scaling both S_1 and S_2 by a common factor leaves it unchanged, so a direct bump-and-revalue at a fixed $\mu^\star$ yields exactly zero delta. The linear-response delta is nonetheless non-zero (-9.25×10^{-6}) because it captures the market recalibration response rather than a frozen-measure revaluation. A spot bump changes the SPX marginals μ_1, μ_2, hence the forward variance σ^2_{fwd}, which propagates to F_V and then to μ_V through the variance anchoring (51). The recalibrated μ^ε reshapes the conditional distribution $P^\varepsilon(S_2 \mid S_1, V)$ to maintain variance consistency, so $\mathbb{E}_{\mu^\varepsilon}[G_{\text{van}}] \neq \mathbb{E}_{\mu^\star}[G_{\text{van}}]$ even though G_{van} is scale-invariant; the resulting non-zero delta therefore reflects the constrained response of the calibrated joint coupling, rather than a direct spot dependence of the payoff.

Payoff agnostic. The dual variation $\dot{\theta}^0 = H^+ h$ is computed once per market scenario and shared across all payoffs. The per-payoff cost is the covariance projection $g_G^\top \dot{\theta}^0$, which is linear in the grid dimension and requires no additional solver call. The framework therefore applies to any structured product on (S_1, V, S_2)—cliquets, corridor variance swaps, forward volatility agreements, or exotic VIX triggers—by computing $g_G = \text{Cov}_{\mu^\star}(G, T)$ and projecting. This is the sense in which the machinery is payoff-agnostic and extends well beyond VIX vanilla options.

10 Conclusion

This paper develops a model-independent framework for SPX–VIX risk generation based on entropic martingale optimal transport. Starting from the joint calibration methodology of Guyon, we show that the calibrated Gibbs coupling admits a natural perturbation theory: admissible market shocks propagate through the Fisher information matrix of the calibrated exponential family, yielding explicit linear-response formulas for risk sensitivities.

To incorporate realistic VIX smile dynamics, we introduce a linearized Skew Stickiness Ratio formulation and use it to determine the VIX marginal target change h_V in the perturbation vector h. This approach allows SPX perturbations to propagate consistently to VIX implied volatility while maintaining the convex structure of the entropic projection problem.

We further show that the perturbed transport problem admits a structural dimensional reduction under a conditional coupling invariance assumption. In this regime the three-dimensional transport problem collapses to a two-dimensional projection on (S_1, V) while preserving the conditional dependence structure inherited from the base calibration. This explains why risk sensitivities can be generated efficiently without re-solving the full martingale optimal transport calibration.

Two sets of numerical experiments support the theoretical framework. First, we compare perturbation-based risk sensitivities with those obtained from full recalibration of the SPX–VIX transport model. Across VIX futures and VIX option cross-greeks, the perturbation method produces sensitivities that are very close to the recalibration benchmark while achieving significant computational speedups. Second, we conduct hedging backtests on randomized VIX option portfolios. Using SPX sensitivities generated by the dimension-reduced transport method, the resulting hedges consistently outperform those based on a stochastic local volatility (SLV) benchmark in terms of hedged P&L variance.

A further consequence of the Fisher-based perturbation structure is that risk generation is *payoff-agnostic*: the linear solve $H\dot{\theta}^0 = h$ depends only on the market shock, not on the payoff. Any derivative contributes only through its covariance vector $g_G = \mathrm{Cov}_{\mu^\star}(G, T)$, computed once at calibration, so the per-Greek cost for each additional instrument reduces to a single projection $g_G^\top \dot{\theta}^0$. The VIX-barrier forward-starting SPX call example makes this concrete: the barrier and vanilla positions share exactly the same Fisher solve, with the barrier's non-trivial cross-delta arising from variance-consistency recalibration rather than any parametric assumption on joint SPX–VIX dynamics.

Overall, the results show that entropic martingale optimal transport provides more than a calibration tool. Combined with perturbation theory and dimensional reduction, it yields a practical framework for SPX–VIX risk generation that is financially consistent, computationally efficient, and effective in hedging applications.

Disclaimer

This paper was prepared for informational purposes in part by the Quantitative Trading & Research Group of JPMorganChase & Co. This paper is not a product of the Research Department of JPMorganChase & Co. or its affiliates. Neither JPMorganChase & Co. nor any of its affiliates makes any explicit or implied representation or warranty and none of them accept any liability in connection with this paper, including, without limitation, with respect to the completeness, accuracy, or reliability of the information contained herein and the potential legal, compliance, tax, or accounting effects thereof. This document is not intended as investment research or investment advice, or as a recommendation, offer, or solicitation for the purchase or sale of any security, financial instrument, financial product or service, or to be used in any way for evaluating the merits of participating in any transaction.

References

Abi Jaber, E., C. Illand, and X. Li (2023). the quintic Orstein–Uhlenbeck volatility model that jointly calibrates SPX & VIX smiles. *Risk*.

Amari, S. (2016). *Information Geometry and Its Applications*. Springer.

Bayer, C., P. K. Friz, G. Fukasawa, Masaaki, A. Jim, Jacquier, and M. Rosenbaum (Eds.) (2023). *Rough Volatility*. Financial Mathematics Series. SIAM.

Beiglböck, M., P. Henry-Labordère, and F. Penkner (2013). Model-independent bounds for option prices: A mass transport approach. *Finance and Stochastics 17*(3), 477–501.

Benamou, J.-D., G. Carlier, M. Cuturi, L. Nenna, and G. Peyré (2015). Iterative bregman projections for regularized transportation problems. *SIAM Journal on Scientific Computing 37*(2), A1111–A1138.

Bergomi, L. (2009, December). Smile dynamics IV. *Risk Magazine 22*(12), 94–100.

Bergomi, L. (2016). *Stochastic Volatility Modeling*. Chapman & Hall/CRC Financial Mathematics Series. Boca Raton: CRC Press.

Black, F. and M. Scholes (1973). The pricing of options and corporate liabilities. *Journal of Political Economy 81*(3), 637–654.

Breeden, D. T. and R. H. Litzenberger (1978). Prices of state-contingent claims implicit in option prices. *Journal of Business 51*(4), 621–651.

Cuchiero, C., G. Gazzani, J. Möller, and S. Svaluto-Ferro (2025). Joint calibration to SPX and VIX options with signature-based models. *Mathematical Finance 35*(1), 161–213.

Cuturi, M. (2013). Sinkhorn distances: Lightspeed computation of optimal transport. *Advances in Neural Information Processing Systems 26*, 2292–2300.

Gatheral, J. (2006). *The Volatility Surface: A Practitioner's Guide*. Hoboken, NJ: John Wiley & Sons.

Guo, I., G. Loeper, J. Obłój, and S. Wang (2022). Joint modeling and calibration of SPX and VIX by optimal transport. *SIAM Journal on Financial Mathematics 13*(1), 1–31.

Guyon, J. (2020, April). The joint S&P 500/VIX smile calibration puzzle solved. *Risk*, 112–117.

Guyon, J. (2024). Dispersion-constrained martingale schrödinger bridges and the exact joint S&P 500/VIX smile calibration puzzle. *Finance and Stochastics 28*(1), 27–79.

Henry-Labordère, P. (2017). *Model-Free Hedging: A Martingale Optimal Transport Viewpoint*. Chapman and Hall/CRC Financial Mathematics Series. CRC Press.

Heston, S. L. (1993). A closed-form solution for options with stochastic volatility with applications to bond and currency options. *The Review of Financial Studies 6*(2), 327–343.

Peyré, G. and M. Cuturi (2019). Computational optimal transport. *Foundations and Trends in Machine Learning 11*(5–6), 355–607.

Rockafellar, R. T. (1970). *Convex Analysis*, Volume 28 of *Princeton Mathematical Series*. Princeton, NJ: Princeton University Press.